ORGANOMETALLICS

pubs.acs.org/Organometallics Article

Planar-Locked Ru-PNN Catalysts in 1-Phenylethanol Dehydrogenation

Paul M. Fanara, Samantha N. MacMillan, and David C. Lacy*

Cite This: *Organometallics* 2020, 39, 3628–3644 Read Online

ACCESS | Metrics & More | Article Recommendations | Supporting Information

ABSTRACT: Ru-PNN pincer catalysts of the general form [{PNN}Ru(H)(Cl)(CO)] can dehydrogenate alcohols through inner- and outer-sphere mechanisms, but determining the favored path is challenging. To address this challenge, the following planar-locked quinoline-based PNN ligands, which cannot form key inner-sphere transition states and intermediates, were synthesized: 2-((ditertbutylphosphaneyl)methyl)-*N*,*N*-diethylquinolin-8-amine (QNP^{tBu}), 2-((diisopropylphosphaneyl)methyl)-*N*,*N*-diethylquinolin-8-amine (QNP^{iPr}), and 2-((diphenylphosphaneyl)methyl)-*N*,*N*-diethylquinolin-8-amine (QNP^{Ph}). In addition to the quinoline-derived ligands, we also prepared the isoquinoline PNN ligand *N*-((1-((di*tert*-butylphosphaneyl)methyl)isoquinolin-3-yl)methyl)-*N*-ethylethanamine (IsoQNP) and two known picoline- and lutidine-derived ligands 2-((di*tert*-butylphosphaneyl)methyl)pyridine (PicP) and 2-((di*tert*-butylphosphaneyl)methyl)-6-methylpyridine (LutP). These six ligands were coordinated to Ru(II) ions to prepare six new complexes of the general formulation [{L}Ru(H)(Cl)(CO)] analogous to Milstein's PNN catalyst precursor (**1PyCl**). The X-ray structural, NMR, UV−vis, and FTIR spectroscopic properties of the new complexes are similar to parent complex **1PyCl** and were used in catalytic 1-phenylethanol acceptor-less and transfer dehydrogenation. The comparative results demonstrate that **1Py** outperforms the other catalysts. DFT reaction profiles were computed for **1Py** and the planar-locked catalysts. The results suggest that **1Py** has access to a lower-energy inner-sphere path, whereas the planar-locked catalysts can only proceed through a high-energy outer-sphere mechanism and may even get trapped in unreactive alkoxide sinks.

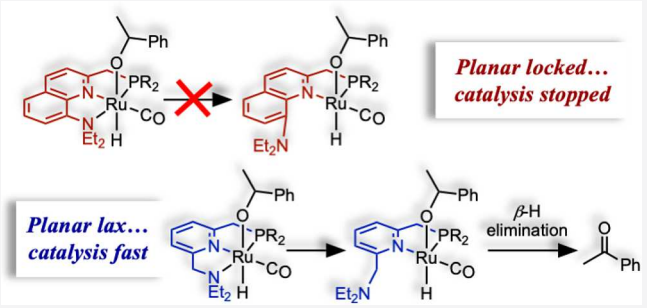

INTRODUCTION

Ruthenium-catalyzed alcohol (de)hydrogenations are important reactions in synthetic organic chemistry.[1−5] A subclass of catalysts are those proposed to rely on aromatization/dearomatization metal ligand cooperative (A/D MLC) substrate activation, as discovered by Milstein and co-workers on Ru-PNN complexes.[6−8] Support for the aromatization/dearomatization comes primarily from early studies where Milstein and co-workers carried out stoichiometric experiments on a 16-e$^-$ Ru-PNN complex (**1Py**).[6,9] Furthermore, several DFT studies provide ample support for the viability of A/D MLC.[10−17] Nevertheless, questions remain. Due to the stated importance in organic synthesis, the versatility and potential atom efficiency of these systems merit further exploration of the reaction mechanism in alcohol dehydrogenation to enable advances in ligand design and applications.

The mechanism of alcohol dehydrogenation can proceed through several conceivable pathways that are generally categorized as being "inner-sphere" or "outer-sphere" in nature (Scheme 1). Outer-sphere dehydrogenation is further delineated into concerted and stepwise mechanisms. The concerted mechanism appears to be relevant for only Shvo-type catalysts,[18] whereas Noyori's catalyst and other pincer systems proceed through stepwise outer-sphere processes.[19−21]

Scheme 1. Key Inner- versus Outer-Sphere Intermediates

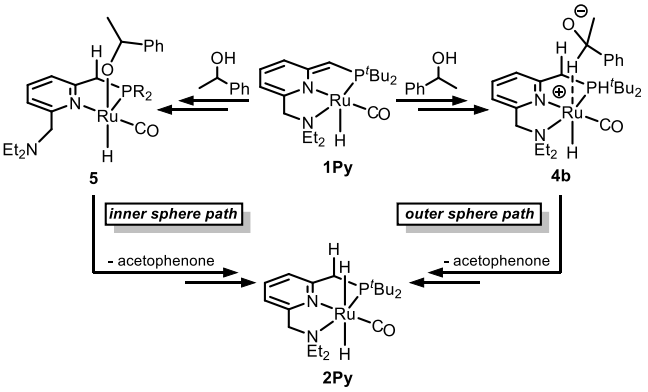

Received: May 9, 2020
Published: October 2, 2020

https://dx.doi.org/10.1021/acs.organomet.0c00327
Organometallics 2020, 39, 3628–3644

Henceforth, we will not consider the concerted process. Although outer-sphere dehydrogenation does not require substrate coordination, the key zwitterionic intermediate (Scheme 1, right) can rearrange into a Ru-alkoxide (Scheme 1, left).[16] Therefore, the observation of Ru-alkoxide complexes under catalytically relevant conditions does not rule out outer-sphere processes.[9,20] In contrast to the outer-sphere mechanisms, the inner-sphere pathway *requires* Ru-alkoxide formation and includes unique steps such as dissociation of an auxiliary ligand arm and a β-hydride elimination of the alkoxide (Scheme 1, left).[10−17]

The known Ru-alkoxide complexes and recent implication of their importance in the mechanism provides a reason to expect competing inner- versus outer-sphere paths in a dehydrogenation reaction. Knowledge of the operative/favored pathway will enable better catalyst design. The challenge is experimentally differentiating these two limiting mechanisms (inner- versus outer-sphere) under catalytic conditions, which is difficult since both can be simultaneously operative and since both key inner- and outer-sphere steps can have large entropies of activation.[22]

While there are many computational studies discussing the viability of inner- versus outer-sphere mechanisms,[10−17] there are very few experimental studies, with Szymczak providing the only example we are aware of for Ru-pincer catalysts and was shown to proceed through the inner-sphere path.[23] This experimental study[23] used an NNN pincer ligand that is fundamentally different from Milstein's PNN system. Nevertheless, the discovery that inner-sphere steps are operative on a Ru-pincer catalyst has implications for the PNN systems.

Further complicating the story is the recent discovery **1Py** can dehydroalkylate into an effective hydrogenation catalyst.[24] In this new finding, the proposed catalytically relevant compound was a Ru(0) imine complex (**1Py^{imine}**), formed through loss of ethane via a phosphine coordination induced dehydroalkylation reaction (Scheme 2), rather than the traditionally thought Ru(II) complex **1Py**. The introduction of a third potential mechanism thus complicates the discussion, reminding us that identification of the active catalyst is not a straightforward endeavor.[20,25,26]

Scheme 2. Formation of 1Py^{imine} [24]

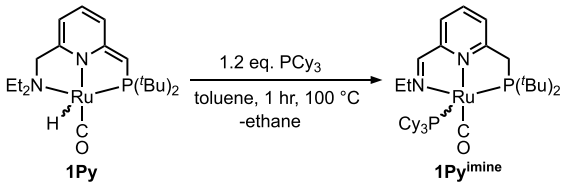

One approach to test these proposed mechanisms is to design ligands that either poison or favor the possible pathways. We envisioned that incorporating a quinoline backbone, instead of a pyridine one, could constrain the system such that the NEt_2-group of the PNN ligand cannot dissociate, which is a requisite step for the inner-sphere pathway. Additionally, the dehydroalkylation steps are negated by removing the required benzylic position. The difficulty in making mechanistic generalizations from ligand changes is that other factors may also contribute to observed differences in reactivity. For example, the changes in aromatic conjugation of a quinoline may significantly alter aromatization/dearomatization thermodynamics. Hence, we also designed and synthesized an isoquinoline analogue to serve as a control for this possibility. Finally, a bidentate PN ligand could, in principle, favor an inner-sphere mechanism; therefore, we additionally prepared new bidentate picoline- and lutidine-derived PN-Ru complexes from known PN ligands for this study (Chart 1).[27,28]

Chart 1. Precatalysts (and Ligands) for This Study[6]

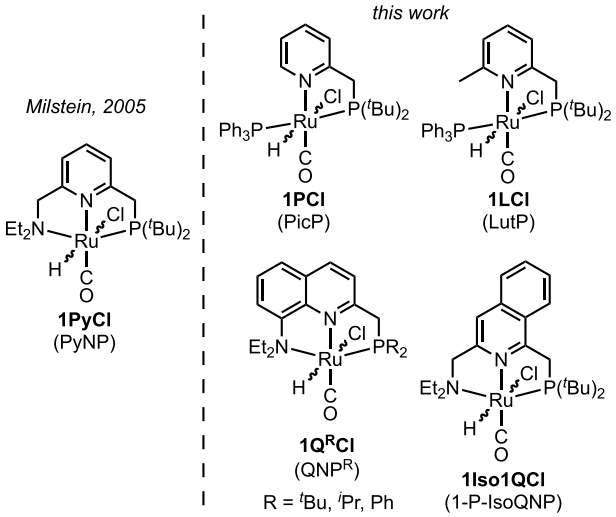

Using both new and known ligands, we prepared the following seven precatalyst complexes: [{PyNP}Ru(CO)(Cl)(H)] (**1PyCl**),[6] [{QNP^R}Ru(CO)(Cl)(H)] (**1Q^{R}Cl**) (R = ^{t}Bu, ^{i}Pr, and Ph), [{1-P-IsoQNP}Ru(CO)(Cl)(H)] (**1Iso1QCl**), [{PicP}Ru(CO)(Cl)(H)(PPh_3)] (**1PCl**), and [{LutP}Ru(CO)(Cl)(H)(PPh_3)] (**1LCl**). These complexes were subjected to a series of experimental catalytic dehydrogenation reactions using 1-phenylethanol (1PhEtOH). The reaction profiles for a variety of mechanisms were studied using DFT with 1PhEtOH as the substrate. Our computational and experimental findings indicate that inhibiting amine arm dissociation negatively impacts the catalytic activity. Collectively, the results allow us to make some reasonable conclusions about the mechanism: The six new complexes likely proceed through an outer-sphere mechanism, and Milstein's catalyst has access to both, with the inner-sphere being favored.

RESULTS

Synthesis of Ligands and Complexes. Unless noted, the ^{t}Bu-substituted phosphine ligands were used in this study. The parent ligand PyNP was synthesized according to literature; many of the steps for the new ligands used these adapted procedures.[6] The picoline- and lutidine-derived ligands PicP and LutP are known,[27,28] but to our knowledge, they have not been used to prepare [{PN}Ru(CO)(H)(Cl)PPh_3] precatalysts.[29]

Synthesis of QNP Ligands. Preparation of the quinoline core for QNP was accomplished via a previously reported Doebner-Miller reaction between crotonaldehyde and 2-nitroaniline to give 8-nitro-2-methylquinoline.[30] The nitro group was reduced quantitatively to the amine using Pd/C and H_2 (gas) (1 atm). This amine product was used without purification in subsequent alkylation using excess $NaBH_4$ in acetic acid to give *N*,*N*-diethyl-2-methylquinolin-8-amine in

https://dx.doi.org/10.1021/acs.organomet.0c00327
Organometallics 2020, 39, 3628−3644

low to moderate yields after column chromatography (Scheme 3).

Scheme 3. Synthesis of QNP Ligands

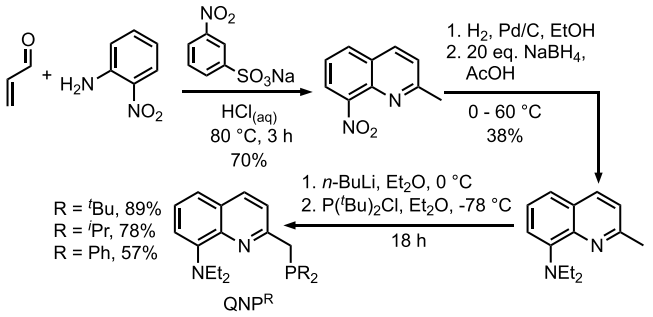

Lithiation of *N*,*N*-diethyl-2-methylquinolin-8-amine with *n*-BuLi at 0 °C and subsequent reaction with $P(^tBu)_2Cl$ at −78 °C installs the $P(^tBu)_2$ group on the 2-methyl position of the quinoline ring giving the final QNP ligand in an overall 24% isolated yield (Scheme 3). We also prepared the diphenylphosphine (QNP^{Ph}) and isopropyl (QNP^{iPr}) derivatives using the same procedure.

Synthesis of IsoQNP. The core isoquinoline unit for 1-P-IsoQNP was prepared through a previously reported procedure in which acetonitrile adds to allyl benzene using silver triflate as a mediator to form 1,3-dimethyl-isoquinoline.[31] Bromination of 1,3-dimethyl-isoquinoline using a procedure similar to that for the parent PyNP ligand[6] yielded two isomers in which either methyl position was brominated, 1-bromomethyl-3-methylisoquinoline and 3-bromomethyl-1-methylisoquinoline. These isomers were separated via column chromatography in somewhat prohibitively low yields (Scheme 4).

Scheme 4. Synthesis of 1-P-IsoQNP Ligand

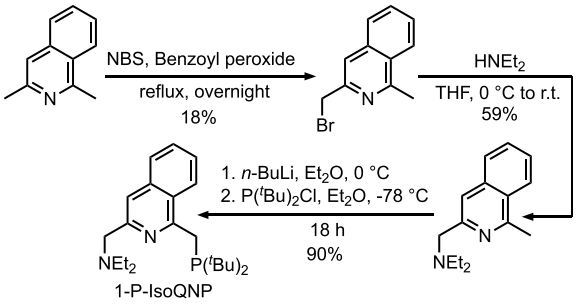

Amination with diethylamine and phosphination followed procedures similar to that for PyNP[6] to give the final IsoQNP ligands. The ligands were named after the position of the phosphorus group on the isoquinoline ring, *N*-((1-((di-*tert*-butylphosphaneyl)methyl)isoquinoline-3-yl)methyl)-*N*-ethylethanamine (1-P-IsoQNP) and *N*-((3-((di-*tert*-butylphosphaneyl)methyl)isoquinoline-1-yl)methyl)-*N*-ethylethanamine (3-P-IsoQNP). 3-P-IsoQNP was not synthesized in reasonable quantities for this current study; therefore, the reactivity is only reported for 1-P-IsoQNP.

Synthesis and Characterization of Ru Precatalysts. Coordination of Ru(II) to the new ligands follows the procedure reported for PyNP (Scheme 5).[6] Specifically, heating a mixture of the desired ligand and $Ru(H)(Cl)(CO)(PPh_3)_3$ to 65 °C in THF in a sealed Schlenk bomb affords the precatalyst compounds. The complexes [{QNP}Ru(H)(Cl)(CO)] (**1QCl**) and [{1-P-IsoQNP}Ru(H)(Cl)(CO)] (**1Iso1QCl**) have $^{31}P\{^1H\}$ NMR ($CDCl_3$) resonances at 111.0 and 107.0 ppm, respectively, and are nearly identical to the reported shift of 108 ppm for the parent complex, **1PyCl**.[6] ^1H NMR ($CDCl_3$) spectra reveals resonances at −15.2 ppm (1H) ($^2J_{PH}$ = 25.9 Hz) for **1QCl** and −15.6 ppm (1H) ($^2J_{PH}$ = 27.7 Hz) for **1Iso1QCl**. These resonances are also near the reported values for the hydride ligand of **1PyCl** (−15.3 ppm, 1H, $^2J_{PH\text{-}cis}$ = 27.50 Hz).[6] ATR FT−IR reveals that the ν(CO) of 1882 cm^{-1} for **1QCl** and 1898 cm^{-1} for **1Iso1QCl** are shifted to a slightly lower energy with respect to the $Ru(H)(Cl)(CO)(PPh_3)_3$ precursor (ν(CO) of 1927 cm^{-1}), just as in parent complex **1PyCl** (1898 cm^{-1}). As stated previously, we also synthesized the ^{i}Pr and Ph variants of the QNP ligands. The coordination of these ligands to $Ru(H)(Cl)(CO)(PPh_3)_3$ followed the same procedure as that for the parent ligands (Scheme 5). The ^{i}Pr and Ph variants of **1QCl**, [{QNP^{iPr}}Ru(H)(Cl)(CO)] (**$1Q^{iPr}Cl$**), and [{QNP^{Ph}}Ru(H)(Cl)(CO)] (**$1Q^{Ph}Cl$**) display $^{31}P\{^1H\}$ NMR ($CDCl_3$) resonances at 100.8 ppm for **$1Q^{iPr}Cl$** and 74.5 ppm for **$1Q^{Ph}Cl$**. Hydride resonances are seen in the ^1H NMR ($CDCl_3$) at −14.8 ppm (1H) ($^2J_{PH}$ = 23.5 Hz) for **$1Q^{iPr}Cl$** and −14.1 ppm (1H) ($^2J_{PH}$ = 26.0 Hz) for **$1Q^{Ph}Cl$**. The ν(CO) of **$1Q^{iPr}Cl$** (1889 cm^{-1}) and **$1Q^{Ph}Cl$** (1909 cm^{-1}) are comparable to that for parent complex **1QCl** (1882 cm^{-1}).

Coordination of the PicP and LutP ligands with $Ru(H)(Cl)(CO)(PPh_3)_3$ in a manner similar to that for QNP and 1-P-IsoQNP affords [{PicP}Ru(H)(Cl)(CO)(PPh_3)] (**1PCl**) and [{LutP}Ru(H)(Cl)(CO)(PPh_3)] (**1LCl**) as the precatalyst systems (Scheme 6). **1PCl** exhibits two doublets in the $^{31}P\{^1H\}$ NMR ($CDCl_3$) spectrum at 98.7 ppm ($^2J_{PP}$ = 277 Hz) and 37.6 ppm ($^2J_{PP}$ = 276 Hz). The ^1H NMR ($CDCl_3$) resonance for the hydride appears at −14.5 ppm (1H) as doublet of doublets ($^2J_{PH}$ = 23.8 and 22.2 Hz). **1LCl** gives a similar resonance pattern, with the hydride in the ^1H NMR ($CDCl_3$) spectrum appearing at −14.8 ppm (1H) as a doublet of doublets ($^2J_{PH}$ = 18.8 and 28.2 Hz). The $^{31}P\{^1H\}$ NMR ($CDCl_3$) spectrum of **1LCl** reveals doublets at 92.3 ppm ($^2J_{PP}$ = 280 Hz) and 35.7 ppm ($^2J_{PP}$ = 280 Hz). The precursor

Scheme 5. Coordination of Ru(II) to Ligands

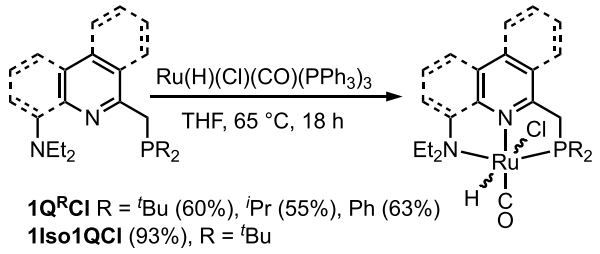

Scheme 6. Coordination of Ru(II) to PicP and LutP

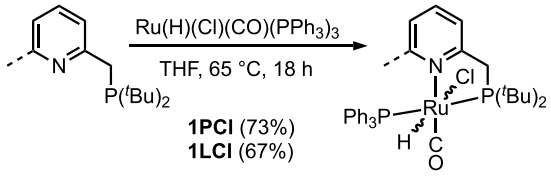

https://dx.doi.org/10.1021/acs.organomet.0c00327
Organometallics 2020, 39, 3628−3644

Table 1. Selected Bond Metrics and Spectroscopic Data of Precatalyst Complexes

complex	ν(CO) (cm^{-1})	Ru−N_{py} (Å)[a]	Ru−L (Å)[b]	Ru−C(Å)	Ru−Cl(Å)	Ru−P (Å)[c]	^{1}H NMRRu−H (ppm)	^{31}P{H} NMR PR_2 (ppm)
1PyCl	1898	2.102(3)	2.260(2)	1.834(3)	2.583(1)	2.2732(8)	−15.6	107.6
1QCl	1882	2.101(2)	2.279(2)	1.842(2)	2.5439(6)	2.2617(6)	−15.2	111.0
1Q^{iPr}Cl	1889	2.095(2)	2.267(2)	1.842(2)	2.5612(7)	2.2393(7)	−14.8	100.8
1Q^{Ph}Cl	1909	2.088(2)	2.255(1)	1.845(3)	2.5594(4)	2.2310(5)	−14.1	74.5
1Iso1QCl	1898	2.111(1)	2.251(1)	1.840(2)	2.5885(5)	2.2525(5)	−15.6	107.0
1PCl	1916	2.184(1)	2.3540(4)	1.841(2)	2.5142(8)	2.3313(5)	−14.5	98.72
1LCl	1924	2.238(2)	2.3624(5)	1.822(2)	2.5468(4)	2.3105(5)	−14.8	92.25

[a]N_{py} represents the nitrogen trans to the CO ligand. [b]L represents either the PPh_3 or NEt_2 trans to the PR_2 ligand. [c]P represents the PR_2 ligand.

complex Ru(H)(Cl)(CO)(PPh_3)$_3$ has a hydride resonance in the ^{1}H NMR ($CDCl_3$) spectrum at −7.2 as a doublet of triplets ($^2J_{PH}$ = 106.4 and 25.3 Hz), with the triplet corresponding to the two PPh_3 ligands cis to the hydride. This assignment and the magnitude of $^2J_{PP}$ allow us to assign **1PCl** and **1LCl** as the cis hydride isomer with PPh_3 trans to the P(^{t}Bu)$_2$ group. As with **1QCl** and **1Iso1QCl**, **1PCl** and **1LCl** display ν(CO) shifted from the starting precursor at 1916 and 1924 cm^{-1}, respectively. A summary of the spectral information on all the complexes reported herein can be found in Table 1.

Unfortunately, the PN-Ru complexes are not directly analogous to **1PyCl** because they have a PPh_3 ligand instead of $RNEt_2$. Attempts were made to replace the PPh_3 ligand with nitrogen-based ligands such as pyridine, acetonitrile, $HNEt_2$, and NEt_3. These syntheses are presently unsuccessful under a variety of conditions and were not pursued further. Notwithstanding, we still proceeded to use the PN-Ru complexes in the reactivity study with 1PhEtOH, but comparative insights are limited, and they were not included in the DFT study.

Structural Characterization of Precatalysts. We obtained and determined the X-ray structures of each of the complexes (Figures 1 and 2). Each complex exhibits a coordination environment similar to that of parent complex **1PyCl** with the exception of **1PCl** and **1LCl**, which have a PPh_3 ligand bound trans to the P(^{t}Bu)$_2$ arm of the ligands. The tridentate ligands are bound in a meridional fashion with the hydride trans to the chloride and cis to the CO ligand. Both enantiomers were found within the unit cell. A summary of the selected bond lengths can be found in Table 1.

Brief Investigation into Generation of 16-e$^-$ Complexes. With precatalyst material in hand, we endeavored to briefly explore the identities of the reactive 16-e$^-$ analogues to **1Py**.[6] First, we confirmed that **1Py** could be formed in our hands. We additionally confirmed Milstein's and Gusev's findings that **2Py** (the Ru-dihydride) is unstable in toluene and slowly converts into **1Py** with the elimination of H_2.[6,20] Notably, this process did not complete within 2 days (∼25% conversion), but it is completed in about 1 h when ≥1 equiv of acetone is included. No effect was observed if catalytic 1PhEtOH was included. These observations will come into play later when we discuss mechanisms.

1QCl can be activated through treatment with KO^{t}Bu in THF at −35 °C forming a dark red (see the Supporting Information for UV−vis spectra) 16-e$^-$ complex [{QNP′}Ru(H)(CO)] (where the ′ symbol denotes a dearomatized ligand) (**1Q**) (Scheme 7) with a ^{31}P{^{1}H} NMR (C_6D_6) signal at 98.7 ppm, close to the literature value of 95 ppm for **1Py**.[6] Furthermore, the formulation of [{QNP′}Ru(H)(CO)] for **1Q** is consistent the ^{1}H NMR resonance at −25.0 ppm ($^2J_{PH}$ = 28 Hz), which is nearly identical to the hydride resonance for **1Py** (−27 ppm and $^2J_{PH}$ = 26 Hz). Retention of the CO ligand is confirmed via a shifted ν(CO) of 1897 cm^{-1}. Following the same procedure for **1Q^{Ph}Cl** also affords a dark red species (**1Q^{Ph}**) with a ^{31}P{^{1}H} NMR (C_6D_6) signal at 61.4 ppm, a ^{1}H NMR resonance at −22.7 ppm ($^2J_{PH}$ = 28 Hz), and ν(CO) at 1905 cm^{-1}.

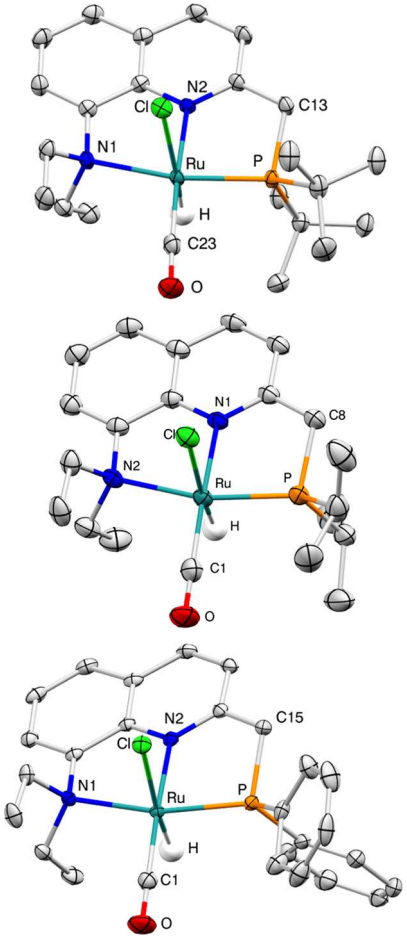

Figure 1. X-ray crystallographically determined molecular structures of one of the molecules found within the unit cell. Shown are **1QCl** (top), **1Q^{iPr}Cl** (middle), and **1Q^{Ph}Cl** (bottom) with ellipsoids at 50% probability; nonhydride H atoms and solvent molecules have been removed for clarity. Color scheme: ruthenium = teal; nitrogen = blue; phosphorus = orange; chloride = lime; oxygen = red; carbon = gray; hydrogen = white.

Clean conversion of **1Iso1QCl** to its corresponding 16-e$^-$ complex was attempted but not achieved in this study. For example, treatment of **1Iso1QCl** with KO^{t}Bu results in a mixture of products, one of which is consistent with **1Iso1Q**

https://dx.doi.org/10.1021/acs.organomet.0c00327
Organometallics 2020, 39, 3628−3644

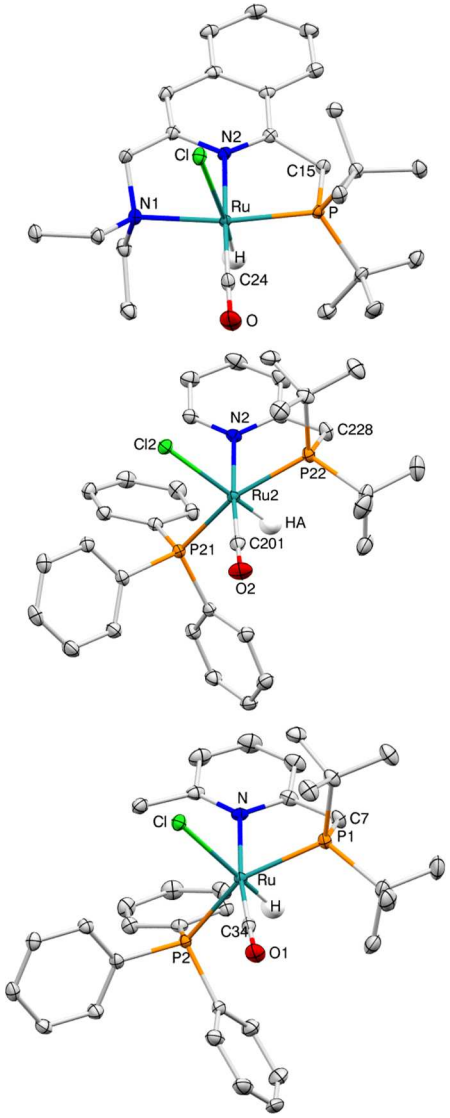

Figure 2. X-ray crystallographically determined molecular structures of one of the molecules found within the unit cell. Shown are **1Iso1QCl** (top), **1PCl** (middle) and **1LCl** (bottom) with ellipsoids at 50% probability; nonhydride H atoms and solvent molecules have been removed for clarity. Color scheme: ruthenium = teal; nitrogen = blue; phosphorus = orange; chloride = lime; oxygen = red; carbon = gray; hydrogen = white.

Scheme 7. Synthesis of 16-e$^-$ Complex 1Q^R[a]

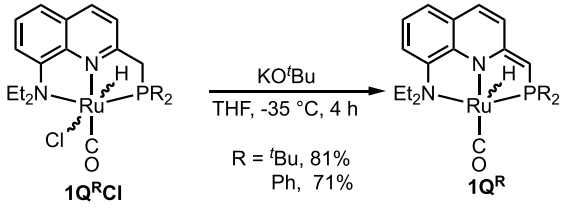

[a]R = ^{t}Bu and Ph.

from its $^{31}P\{^1H\}$ NMR (C_6D_6) peak at 95 ppm and a ^1H NMR resonance at −26 ppm with $^2J_{PH}$ = 26 Hz, but it rapidly decomposes and is one species among many (Figure S56−57). In addition to ligand synthesis difficulties, this constitutes one reason we did not pursue the isoquinoline systems in detail. We note this instability of **1Iso1Q** later within the context of catalysis.

Activation of **1PCl** with KO^{t}Bu in THF at −35 °C appears to form a species that we are tentatively assigning as [{PicP′}Ru(*trans*-$(PPh_3)_2$)$(CO)_2$]$^+$ along with other byproducts (Scheme 8). The assignment of [{PicP′}Ru(*trans*-$(PPh_3)_2)(CO)_2]^+$ is based on $^{31}P\{^1H\}$ NMR spectrum having a triplet at 88.7 ppm ($^2J_{PP}$ = 105.6 Hz) and a doublet at 49.2 ppm ($^2J_{PP}$ = 104.8 Hz) (Figure S59). Furthermore, the ^1H NMR spectrum lacks a hydride resonance (Figure S58), and ATR FT−IR spectra show the presence of two ν(CO) at 1850 and 1887 cm^{-1}. We explored several alternative reactants and conditions, but so far we have not been successful in preparing an analogous 16-e$^-$ complex to **1Py** with **1PCl**.

Scheme 8. Reaction Between 1PCl and KO^{t}Bu

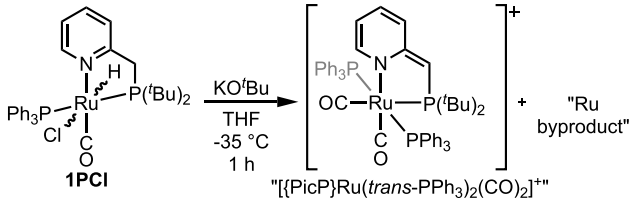

In contrast, activation of **1LCl** with KO^{t}Bu in toluene or THF results in formation of a green species (**1L**) (Scheme 9, Figures S52−S54) whose formulation is consistent with [{LutP′}Ru(CO)(*cis*-H)(PPh_3)] on the basis of a hydride resonance in the ^1H NMR spectrum at −14.3 ppm with $^2J_{PH}$ (doublet of doublets) = 19 and 23 Hz. $^{31}P\{^1H\}$ NMR reveals two doublets at 118.2 ppm ($^2J_{PP}$ = 234.7 Hz) and 54.8 ppm ($^2J_{PP}$ = 234.0 Hz). A ν(CO) was observed at 1881 cm^{-1}, which is shifted from the starting complex **1LCl**. This spectroscopic data is consistent with the *cis*-H *trans*-bisphosphine isomer (Scheme 9).

Scheme 9. Reaction Between 1LCl and KO^{t}Bu

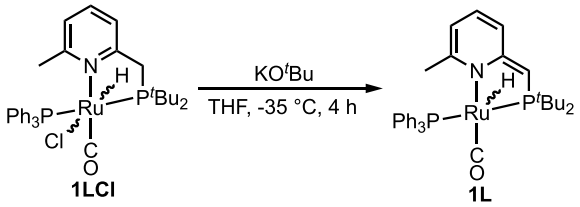

Catalytic Dehydrogenation Reactions. Having established that the PN and PNN-Ru precatalysts behave similarly to parent **1PyCl** with KO^{t}Bu in toluene and THF, we conducted a catalytic study using these seven Ru precatalysts (**1PyCl**, **1Q^{R}Cl** (R = ^{t}Bu, ^{i}Pr, and Ph), **1Iso1QCl**, **1PCl**, and **1LCl**) in dehydrogenation reactions of 1PhEtOH and 1-hexanol (Scheme 10, Table 2). Only **1PyCl** and **1Py** dehydrogenated 1-hexanol. The choice of 1PhEtOH was made in part because of the difficulty these catalysts have in its conversion to acetophenone, and therefore allows us to better

Scheme 10. Dehydrogenation of 1PhEtOH in Toluene

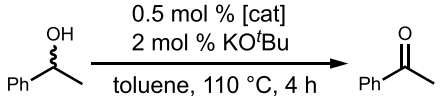

https://dx.doi.org/10.1021/acs.organomet.0c00327
Organometallics 2020, 39, 3628−3644

Table 2. Summary of Dehydrogenation and Transfer Dehydrogenation Reactions in Toluene[a]

			conv (%)[c]	
entry	complex	base (4 equiv)	non-TD	TD[b]
1	**1Py**[d]	none	43 ± 3	
2	**1PyCl**	KO^{t}Bu	43 ± 7	89 ± 5
3	**1Q**[d]	none	1 ± 1	
4	**1QCl**	KO^{t}Bu	4 ± 2	4 ± 1
5	**1Q^{iPr}Cl**	KO^{t}Bu	5 ± 3	50 ± 1[e]
6	**1Q^{Ph}Cl**	KO^{t}Bu	9 ± 5	14 ± 3
7	**1Iso1QCl**	KO^{t}Bu	11 ± 2	11 ± 1
8	**1PCl**	KO^{t}Bu	21 ± 2	88 ± 10
9	**1LCl**	KO^{t}Bu	24 ± 5	88 ± 1
10	Ru[f]	KO^{t}Bu	13 ± 2	29 ± 16
11	none	KO^{t}Bu	0	0
12	none	none	0	

[a]Conditions: 0.5 mol % catalyst, 2 mol % base (if specified), 2 mL of toluene, 0.83 mmol of substrate, 110 °C, 4 h.[32] [b]After adding 1 mL of acetone. [c]Conversions to acetophenone were calculated using ^{1}H NMR using the peaks associated with starting substrate and acetophenone (see the Experimental Section for details), performed in triplicate. [d]Prepared *ex situ*. [e]Average of two runs. [f]Ru = Ru(H)(Cl)(CO)(PPh$_3$)$_3$.[33,34]

make comparisons between the ligands (if each catalyst quantitatively converted the substrate, comparisons would be challenging). Additionally, acetophenone is not prone to the dehydrogenative coupling, so efficiencies of secondary reactions occurring after initial dehydrogenation steps will not complicate our comparison. As will be described in the "Discussion" section, we suspected that poor conversions were due to a competitive transfer hydrogenation reaction with acetophenone (reverse reaction). Therefore, we also conducted transfer dehydrogenation (TD) reactions with acetone and the aforementioned catalysts (Table 2).

Density Functional Theory Study. We performed a DFT study of the activated complexes in Chart 1, with the exception of **1P** and **1L**,[35] for both inner-sphere and stepwise outer-sphere mechanisms for dehydrogenation with 1PhEtOH (Schemed 11 and 12) (see the Experimental Section for details). A different methodology was used for **Iso1Q** and is not considered further (see the Supporting Information).

Summary of Computed Stepwise Outer-Sphere Mechanism. The outer-sphere dehydrogenation mechanism (Scheme 11, Figure 3, red) starts with an approach of 1PhEtOH to **1Py** in a side-on fashion forming transition state **TS$_{OS\text{-}PT}$** ($\Delta G^{\ddagger}$ = 21.2 kcal/mol) and involves substrate proton transfer to the dearomatized ligand. The resulting intermediate **4bPy** is a zwitterionic-sigma complex linked through the C−H bond of the substrate to the Ru center (ΔG° = 20.6 kcal/mol). This high-energy intermediate (**4bPy**) can readily transfer a hydride to the ruthenium center through **TS$_{OS\text{-}HT}$** ($\Delta G^{\ddagger}$ = 2.7 kcal/mol) to form acetophenone and known dihydride complex **2Py** (ΔG° = 1.9 kcal/mol).[6] Alternatively, **4bPy** can isomerize to alkoxide **4aPy** through **TS$_{4b\text{-}4a}$** ($\Delta G^{\ddagger}$ = 2.9 kcal/mol) (Figure 3, purple), thereby connecting the outer- and inner-sphere mechanisms. Elimination of H$_2$ from **2Py** is discussed later. This mechanism was also computed for each active species in Chart 1 with the exception of **1P** and **1L** (Figures 7, S1, S60).[35]

Summary of Computed Inner-Sphere Mechanism. The first step in the inner-sphere dehydrogenation mechanism (Scheme 11, Figure 3, blue) is coordination of 1PhEtOH to **1Py** to form **3Py** (ΔG° = 9.2 kcal/mol). Following the coordination, a proton transfer to the methylene carbon on the ligand (**TS$_{In\text{-}PT}$**) ($\Delta G^{\ddagger}$ = 18.4 kcal/mol) produces alkoxide intermediate **4aPy**. The benzyl alcohol derivative of this species was observed by Milstein at low temperature,[9c] and Gusev has characterized the ethoxide complex (analogous to **4aPy** in Scheme 11) under catalytically relevant conditions.[20,19] Collectively, these results agree with our DFT results that the alkoxide complex is in a well of the overall inner-sphere reaction coordinate (ΔG° = 10.3 kcal/mol, Figure 3).

The next process in the inner-sphere mechanism is an NEt$_2$-arm dissociation (**TS$_{4a\text{-}5}$**). Note that there are a number of factors increasing the NEt$_2$ arms' lability. Namely, the trans effect from −P^{t}Bu$_2$ and the cis effect from the alkoxide are both expected to enhance the lability of the NEt$_2$ arm. As such, the barrier for dissociation of the NEt$_2$ arm is low (**TS$_{4a\text{-}5}$**) ($\Delta G^{\ddagger}$ = 1.8 kcal/mol), and the transition state vibration resembles the motion expected for pyramidal inversion rather than an "arm swing" (Figure S3). After dissociation, a vacant site for β-hydride elimination becomes available on 16-e$^-$ intermediate **5Py** (ΔG° = 10.9 kcal/mol). The β-hydride elimination step occurs through a four-centered transition state (**TS$_{In\text{-}HT}$**) ($\Delta G^{\ddagger}$ = 5.4 kcal/mol) resulting in release of acetophenone and *cis*-dihydride complex **6Py** (ΔG° = 14.5 kcal/mol). Isomerization

Scheme 11. Computed Inner-Sphere (Blue) and Stepwise Outer-Sphere Mechanisms[a]

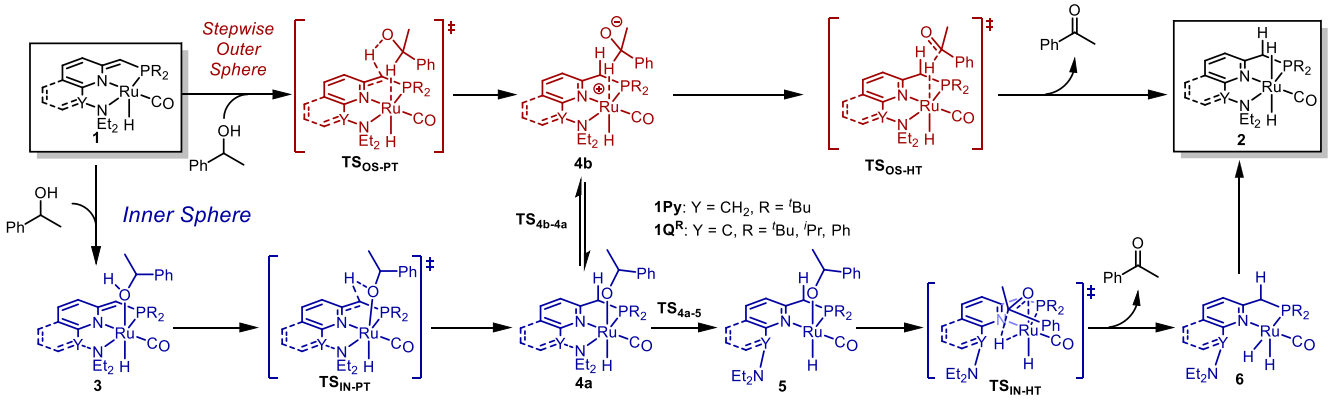

[a]Inner-sphere, blue; outer-sphere, red.

https://dx.doi.org/10.1021/acs.organomet.0c00327
Organometallics 2020, 39, 3628−3644

Scheme 12. Computed Pathways for H_2 Release[a]

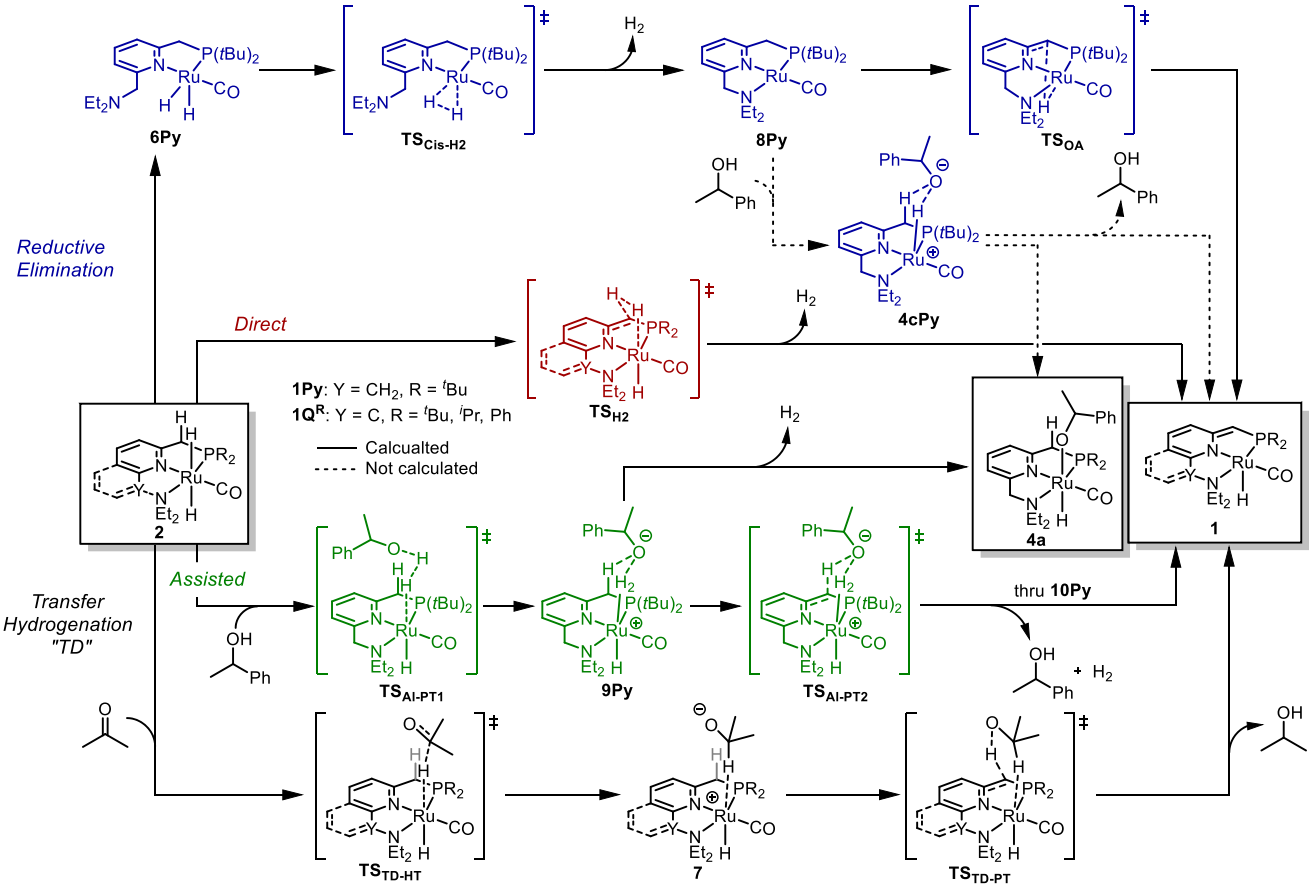

[a]Reductive elimination (blue) direct (red), alcohol-assisted (green), and TD (black).

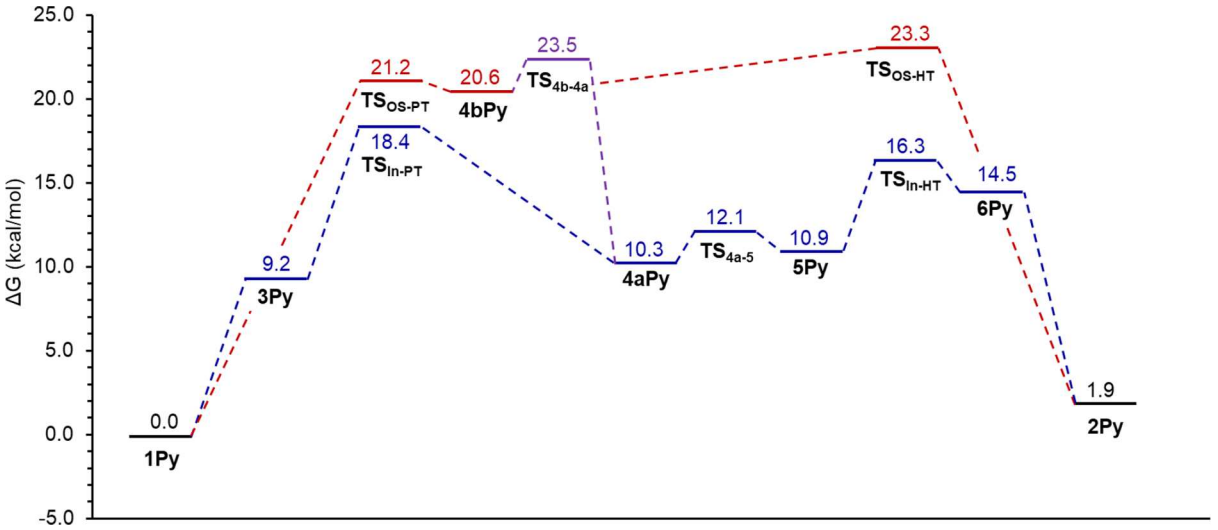

Figure 3. Computed stepwise outer-sphere (red) and inner-sphere (blue) mechanisms of dehydrogenation with **1Py** (see Scheme 11).

of the *cis*-dihydride to *trans*-dihydride complex **2Py** was optimized as a single step wherein the N arm coordinates during isomerization.

Importantly, the ability for $\mathbf{1Q}^{tBu/iPr/Ph}$ to dissociate the amine ligand is significantly diminished to the point that it is not relevant, and complexes $\mathbf{5Q}^{tBu/iPr/Ph}$ and $\mathbf{TS_{In}Q}^{tBu/iPr/Ph}$ could not be optimized *in silico*. We interpret this as support for our hypothesis that it is unreasonable for $\mathbf{1Q}^{tBu/iPr/Ph}$ to perform dehydrogenation via an inner-sphere mechanism. This mechanism was also computed for each active species in Chart 1 with the exception of **1P** and **1L** (Figures 3, 7, and S60).[35]

Summary of H_2 Elimination. **2Py** can eliminate H_2 through several potential pathways; seven of these are discussed (Scheme 12, Figure 4) below:

(1) H_2 can be eliminated directly in a unimolecular dearomatization MLC step ($\mathbf{TS_{H2}}$ $\Delta G^{\ddagger}$ = 25.8 kcal/mol,

https://dx.doi.org/10.1021/acs.organomet.0c00327
Organometallics 2020, 39, 3628−3644

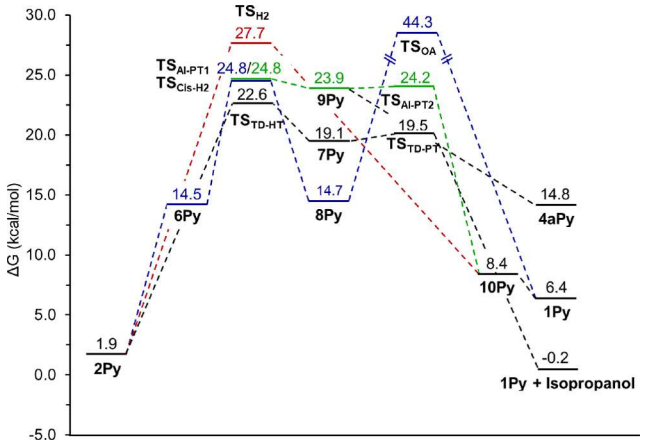

Figure 4. Computed direct (red), reductive elimination (blue), alcohol-assisted (green), and TD (black) mechanisms of H_2 release from **2Py** (see Scheme 12).

relative to **2**) (Scheme 12, Figure 4, red) and is referred to as the "direct" mechanism.

(2) **2Py** can dissociate the NEt_2 arm and isomerize to *cis*-dihydride **6Py** (ΔG° = 14.5 kcal/mol, Figure 4, blue), wherein **6Py** reductively eliminates H_2 to form a Ru(0) complex **8Py** (ΔG° = 14.7 kcal/mol) through $\mathbf{TS_{Cis\text{-}H2}}$ ($\Delta G^\ddagger$ = 10.3 kcal/mol). **1Py** can be reformed through an intramolecular oxidative addition across the C−H on the ligand ($\mathbf{TS_{OA}}$, $\Delta G^\ddagger$ = 29.6 kcal/mol) (Scheme 12, Figure 4, blue). As this pathway contains an unreasonably high barrier energy of 29.6 kcal/mol, it is unlikely to be the pathway for H_2 release. A similar high transition state was computed for an OA step ($\Delta G^\ddagger$ = 41.6 kcal/mol unassisted) for an analog to Milstein's catalyst, and it was similarly concluded that this is not a reasonable path.[36]

(3) Another possible fate of Ru(0) species **8Py** is OA of an alcohol. A concerted OA would result in an axial CO position (as opposed to the usual basal position). Stepwise alcohol OA would likely initiate with metal protonation, forming cationic [{PyNP}Ru(II)(CO)(H)][OR] (**4c**), similar to species **4b**. The outer-sphere alkoxide in **4c** could deprotonate the methylene arm resulting in free alcohol and reforming of **1Py** through a transition state much like $\mathbf{TS_{TD\text{-}PT}}$ and $\mathbf{TS_{OS\text{-}PT}}$. Another possibility is that the alkoxide could migrate to a coordination site trans to the hydride resulting in formation of **4a**, essentially isomerizing through a transition state like $\mathbf{TS_{4b\text{-}4a}}$. This process would bypass **1Py** and close the cycle. Given the similarities of these TS and intermediates to those already computed, none of these paths were computed but they are possible and represent a potential lower path than the "direct" H_2 elimination step.

(4) In the presence of an "H_2" acceptor such as acetone, **2Py** can lose "H_2" via a transfer hydrogenation of acetone (Scheme 12, Figure 4, black). Transfer of the hydride to acetone proceeds through $\mathbf{TS_{TD\text{-}HT}}$ ($\Delta G^\ddagger$ = 20.7 kcal/mol) and results in zwitterionic sigma complex **7Py** (ΔG° = 19.1 kcal/mol). Proton transfer from the ligand to the isopropoxide via $\mathbf{TS_{TD\text{-}PT}}$ ($\Delta G^\ddagger$ = 0.4 kcal/mol) results in reformation of **1Py** and release of isopropanol.

(5) TD can also occur by an inner-sphere mechanism for **1Py**, which shares identical steps to the reverse of inner-sphere dehydrogenation of 1PhEtOH except that the phenyl is substituted for a methyl (blue line in Figure 3), so it was not computed.

(6) A sixth possibility is the "alcohol-assisted mechanism". In such a mechanism, a catalytic 1PhEtOH molecule transfers its O−H proton to the hydride ($\mathbf{TS_{Al\text{-}PT1}}$) ($\Delta G^\ddagger$ = 24.8 kcal/mol), generating an H_2 adduct with an alkoxide counterion (**9Py**) (ΔG° = 23.9 kcal/mol) (Scheme 12, green). This is followed by deprotonation of the ligand by the alkoxide ($\mathbf{TS_{Al\text{-}PT2}}$) ($\Delta G^\ddagger$ = 0.3 kcal/mol) resulting in release of 1PhEtOH and the H_2 adduct of **1Py** (**10Py**) (ΔG° = 8.4 kcal/mol). Dissociation of H_2 regenerates **1Py**.

It should be noted that a catalytic ROH acceptor/donor (e.g., ethanol, 1PhEtOH, *tert*-butanol, water, etc.) can change the barrier for any step involving the transfer of a hydrogen nucleus through ROH assistance.[12,17,19,20,37,38] Experimentally, the energy change can be as much as 5 kcal/mol for the associated $\Delta G^\ddagger$ when including H-bond acceptor/donor for proton shuttling.[39] These paths are stepwise, with computed concerted paths now recognized to be artifacts of gas-phase optimizations.[40]

(7) Alternatively, the alkoxide in **9Py** can displace H_2 to form the previously mentioned coordinated alkoxide intermediate **4aPy**, which can undergo dehydrogenation via an inner-sphere pathway. This mode of H_2 release is notably unique in that it bypasses the regeneration of **1Py** allowing for a mechanism that is completely free of aromatization/dearomatization steps altogether. Gusev has studied this process and demonstrated that both routes, A/D MLC and non-A/D MLC, are viable.[20]

While there are many possible H_2 elimination pathways, it is noteworthy that the lower energy paths involve catalytic substrate or a sacrificial acceptor molecule (acetone) and that the highest energy paths are unimolecular. In fact, some proposed paths indicate autocatalytic behavior (alcohol-assisted paths).[41] In part, the complexity afforded from these many H_2 elimination pathways is what makes differentiating inner- versus outer-sphere mechanisms difficult. Testing these various paths is *not part of this study*, which is focused on amine arm dissociation inhibition through planar-locked Ru pincer complexes.

■ DISCUSSION

There are several conceivable mechanisms involved in the dehydrogenation of alcohols with Ru-PNN pincer catalysts. One of these includes the *concerted* outer-sphere mechanism. This process has a single transition state exemplified in Shvo's catalyst.[18] Others have recently shown that the concerted mechanism in (de)hydrogenations is not feasible for other systems and instead proceed via *stepwise* outer-sphere mechanisms. This has been demonstrated for Ru-PNN pincer complexes such as **1Py**.[19,20] The stepwise mechanism breaks the transfer of the two H-nuclei into two separate steps with a high-energy zwitterionic sigma complex intermediate (Int 5 in ref 20; **4bPy** here). As a high-energy intermediate, this zwitterionic sigma complex may collapse into an O-bound Ru-alkoxide (Int 4 in ref 20; **4aPy** here). Hence, the observation of Ru-alkoxide species under catalytically relevant conditions is fully consistent with *both* outer- and inner-sphere pathways. The inner-sphere path involves a key dissociation step of an auxiliary ligand-arm from a Ru-alkoxide complex to create a vacant coordination site that is followed by beta-hydrogen elimination (Scheme 11, blue). Differentiating these inner- and

https://dx.doi.org/10.1021/acs.organomet.0c00327
Organometallics 2020, 39, 3628−3644

outer-sphere paths, either experimentally and computationally, has been a challenge.

A classic way to differentiate these operative mechanisms is to use kinetic isotope effects (KIE). For instance, Casey demonstrated the viability of a concerted mechanism on Shvo's catalyst using KIE and stands as one of the only bona fide examples of such a concerted transfer.[22] Following similar strategies, Szymczak demonstrated that the inner-sphere path is the mechanism in 1PhEtOH dehydrogenation on a Ru-NNN system.[23] As with any mechanism, it is likely that multiple paths are occurring with one being favored over the others and constitutes one reason that KIE can be difficult to interpret. Instead, it is our intention that by using planar-locked, quinoline-derived Ru-PNN complexes (Chart 1) some clues as to the favored path can be discovered. The variations and properties of the complexes are briefly discussed immediately below, and then a discussion regarding our experimental and DFT comparison follows.

Structural Comparisons. We prepared the new precatalyst complexes and characterized them with a battery of typical spectroscopic techniques. Overall, the spectroscopic and structural properties are similar to the parent **1PyCl** system published by Milstein and co-workers (Table 1).[6] However, a few notable differences are observed and best described pictorially (Figure 5). Of note is the "tilt" (Θ) of the Cl−Ru

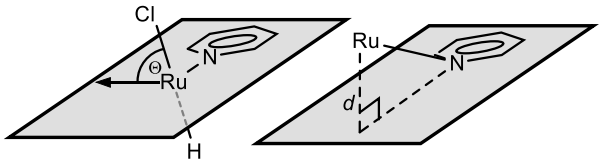

Complex	Θ (°)
1QCl	89
1Q^{iPr}Cl	83
1Q^{Ph}Cl	77
1Iso1QCl	70
1PyCl	68
1PCl	52
1LCl	51

Complex	*d* (Å)
1LCl	0.316
1Q^{Ph}Cl	0.269
1Iso1QCl	0.207
1Q^{iPr}Cl	0.167
1PCl	0.148
1QCl	0.117
1PyCl	0.057

Figure 5. The "tilt" angle Θ (left), defined as the angle between the Cl−Ru bond and the plane formed by the pyridine ring, and the deviation from displacement of the Ru atom from the same plane (*d*) (right) were determined from crystallographic measurements of the precatalysts; each parameter is listed in decreasing magnitude.

bond with respect to the plane formed by the pyridine ring. This parameter can be thought of as a combination of the steric bulk from the substituted phosphine and the geometry imposed by the specific PNN ligand. The efficiency of 1PhEtOH dehydrogenation correlates well with this angle, with the exception of **1PyCl** (Figure 6). Although interesting, this correlation may have little to no implications on the mechanism, but it does visually indicate that **1PyCl** is unique compared to the other six precatalysts. The other notable structural difference is the displacement (*d*) of the Ru atom from the plane formed by the pyridine ring.[42]

Reactivity Comparisons. With the exception of parent catalyst **1PyCl**, our finding is that the other six complexes (**1Q$^{tBu/iPr/Ph}$Cl**, **1Iso1QCl**, **1PCl**, and **1LCl**) and the Ru precursor Ru(H)(Cl)(CO)(PPh_3)$_3$ are poor catalysts for the

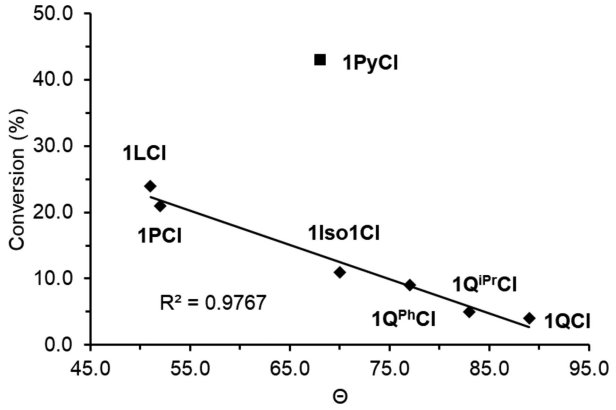

Figure 6. Dehydrogenation conversion plotted against Θ (see Figure 5) for **1LCl**, **1PCl**, **1Iso1QCl**, and **1Q^{R}Cl** (R = ^{t}Bu, ^{i}Pr, and Ph).

dehydrogenation of 1PhEtOH (Table 2).[32] There are several possible explanations.

One possible explanation is that dearomatized 16-e$^-$ complexes analogous to **1Py** cannot form or are not catalytically relevant. For instance, even though **1Q**, **1Q^{Ph}**, and **1L** are stable complexes, **1Q** prepared independently was not as active as **1Q** prepared *in situ* using **1QCl** and base (Table 2, entries 3 and 4). In contrast, **1Py** prepared independently or *in situ* from **1PyCl** and base functioned the same in 1PhEtOH dehydrogenation (Table 2, entries 1 and 2). However, analogous **1Iso1Q** and **1P** compounds were unstable, but nevertheless the associated precatalysts outperformed **1Q^{R}Cl** in acceptor-less 1PhEtOH dehydrogenation catalysis. Thus, the different catalytic performances cannot be directly related to the different reactivities of the 16-e$^-$ complexes. Additionally, the 16-e$^-$ complexes may not be the active catalysts. Instead, dihydride **2Py** may act as the catalyst. However, the implication of this is not studied herein.

A second possible explanation for the different reactivity is that **1Py** or **2Py** is not involved in 1PhEtOH dehydrogenation and that some other intermediate uniquely accessible to Milstein's catalyst is involved. For instance, Keith and Chianese and co-workers showed that in the presence of PCy_3, **1Py** dehydroalkylates into catalytically relevant complex **1Py^{imine}** (Scheme 2).[24] The quinoline- and bidentate pyridine/lutidine-derived systems cannot dehydroalkylate, serving as one possible explanation for the observed poor catalysis. However, the isoquinoline complex (**1Iso1Q**) *can* dehydroalkylate, but it was similarly not very effective. Unfortunately, the relevance of the dehydroalkylated species cannot be inferred here, especially since dehydroalkylation required exogenous phosphine.[24]

A third explanation for the different reactivity is that **1Py** has access to a low-energy inner-sphere path that the other six catalysts cannot access. For example, **Q^{R}** systems are unable to perform inner-sphere dehydrogenation because they are planar-locked. Since these catalysts cannot operate through an inner-sphere mechanism, they are likely proceeding through an outer-sphere mechanism. Anecdotally, our limited efforts to chemically induce dissociation of PPh_3 from **1L**, **1LCl**, and **1PCl** were unsuccessful (*vide supra*) indicating inert dissociative properties.

Transfer Dehydrogenation Studies. We confirmed that **1PyCl** and **1Py** were effective catalysts for 1-hexanol dehydrogenative coupling to ensure our methodology

https://dx.doi.org/10.1021/acs.organomet.0c00327
Organometallics 2020, 39, 3628−3644

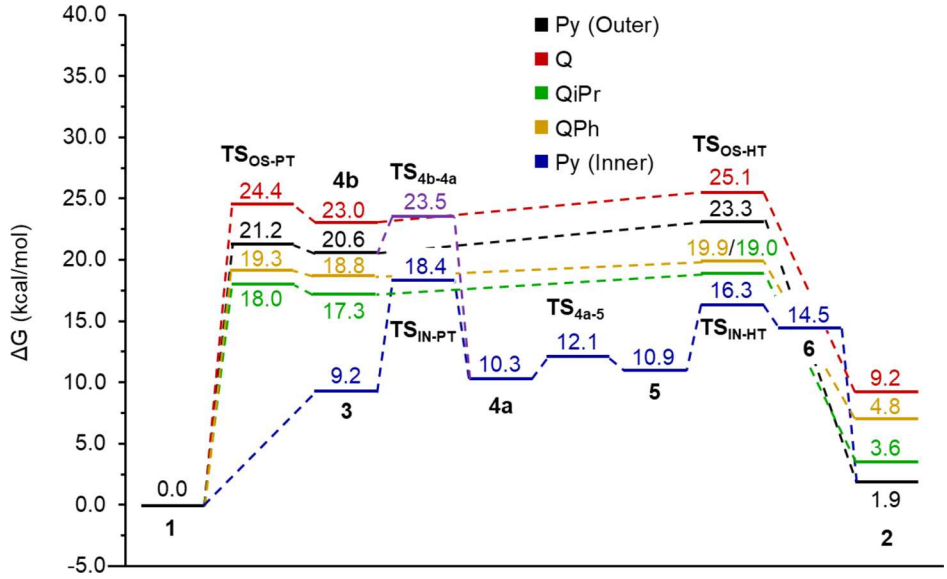

Figure 7. Computed mechanisms of dehydrogenation with **1Py** (outer-sphere (black) and inner-sphere (blue)) and $\mathbf{Q}^{R}$ (R = ^{t}Bu (red), ^{i}Pr (green), and Ph (yellow)) (see Schemes 11 and 12 for mechanism pathways).

(quantitative conversion to hexyl hexanoate under identical conditions in Table 2).[6] Hence, the incomplete dehydrogenation of 1PhEtOH with **1PyCl** (43:57 mixture of product to substrate) suggested that an equilibrium is being established with acetophenone. We tested this by performing the dehydrogenation reaction with a 50:50 mixture of product/substrate, and this ended at a 60:40 mixture (10% conversion). We also charged normal catalytic runs with additional 1PhEtOH after the yield plateaued and observed the ratio ended at 40:60. Together, these suggest that the system approaches an equilibrium with acceptor-less dehydrogenation initially occurring until eventually evolution of H_2 from **2Py** cannot outcompete the backward reaction with acetophenone. We isolated **2Py** and found that it converts slowly at room temperature into **1Py** with loss of H_2 in benzene (54 h, 25% conversion), consistent with our own DFT and literature.[6,20] However, **2Py** converted into **1Py** in just over 1 h if treated with acetone.[41] These results support multiple dihydride-dehydrogenation pathways for **2Py** and are fully consistent with our DFT computations (*vide infra*).

When acetone was included in the reaction, conversions were dramatically improved, even for some of the catalysts that otherwise were ineffective for acceptor-less 1PhEtOH dehydrogenation (Table 2). For example, **1PCl** and **1LCl** catalytically convert 1PhEtOH on par with **1PyCl** with 88% conversion and $\mathbf{1Q^{iPr}Cl}$ had nearly a 10-fold increase. A small increase in conversion was observed for Ru(H)(Cl)(CO)-$(PPh_3)_3$ (29% conversion),[34] while **1Iso1QCl**, **1QCl**, and $\mathbf{1Q^{Ph}Cl}$ were largely unaffected.

Insights from Computations. The inner-sphere mechanism could not be calculated for the quinoline catalysts, $\mathbf{Q}^{R}$ (R = Ph ^{i}Pr, and ^{t}Bu). While this is not definitive evidence that the $\mathbf{Q}^{R}$ system cannot dehydrogenate through an inner-sphere pathway, it does provide a good basis that the quinoline catalysts are proceeding through an alternative pathway. One of these alternatives is the outer-sphere mechanism. Evidence for this path may be found by observing the effect of steric bulk on $\mathbf{Q}^{R}$ catalysts. For example, increasing steric bulk in $\mathbf{Q}^{R}$ (R = ^{i}Pr < ^{t}Bu) resulted in less conversion within 4 h (Table 2). The DFT computed outer-sphere $\Delta G^{\ddagger}$ for $\mathbf{TS_{OS\text{-}PT}}$ (in kcal/mol) are 18.0 and 24.4 for R = ^{i}Pr and ^{t}Bu, respectively, and these are consistent with the observed catalytic performance, $\mathbf{Q^{iPr}} > \mathbf{Q^{tBu}}$. While this does not provide definitive evidence, an outer-sphere mechanism is expected to be inhibited by steric bulk. Therefore, it is reasonable to assume that an outer-sphere mechanism is operative for $\mathbf{Q}^{R}$ catalysts.

In comparing the reaction coordinates between the **Py** and $\mathbf{Q}^{R}$ systems, it is apparent that the inner-sphere path is more favorable (Scheme 11 and Figure 7, blue). Dihydride **2** is the most stable complex along the reaction coordinate and there are several conceivable paths forward (*vide supra*). Furthermore, **2Py** can even proceed through inner-sphere TD paths that the $\mathbf{Q}^{R}$ system does not have access to (reverse of blue mechanism in Figure 7, but with acetone instead of acetophenone).

An additional point regarding the poor performance of the $\mathbf{Q}^{R}$ system is that of the alkoxide intermediates. The zwitterionic intermediate (**4b**) can isomerize to the alkoxide complex (**4a**) (Figure 7, $\mathbf{TS_{4b\text{-}4a}}$). Gusev has calculated this barrier to be 3.7 kcal/mol with an ethanol derivative of **4bPy** (Int **5**, ref 20). Our calculations show this barrier ($\mathbf{TS_{4b\text{-}4a}}$) to be 2.9 kcal/mol, which is in competition with $\mathbf{TS_{OS\text{-}HT}}$ ($\Delta G^{\ddagger}$ = 2.7 kcal/mol).

As such, it is likely that the quinoline derivatives of **4b** could be isomerizing to **4a**. For the **Py** system, this is not an impedance because the alkoxide species is an intermediate that lies directly on an accessible inner-sphere pathway. In contrast, the planar-locked catalysts (i.e., $\mathbf{Q}^{R}$) and those with inert PPh_3 ligands (i.e., **1L** and **1P**) must proceed through high-energy transition states and intermediates with Ru-bound alkoxides being off-path intermediates.

Limitations in Mechanistic Insight. The mechanistic landscape of any system is expected to be complicated; therefore, the results of this study should be considered with this in mind. Mechanisms can change dramatically with small changes in ligand structure, conditions, and substrate. We attempted to control for ligand structure changes by including isoquinoline (**1IsoQ1Cl**) and bidentate (**1PCl** and **1LCl**) systems. These had marginally better efficiencies than the $\mathbf{Q}^{R}$ system in acceptor-less dehydrogenation but were otherwise

https://dx.doi.org/10.1021/acs.organomet.0c00327
Organometallics 2020, 39, 3628−3644

similarly behaved (Figure 6); thus, they have limited value in drawing conclusions about mechanisms. Additionally, there are other possible mechanistic paths and/or caveats that we did not fully explore in this work. (a) For instance, the role of base was not considered in this study. While both **1Py** and **1PyCl** functioned the same in 1PhEtOH dehydrogenation (Table 2, entries 1 and 2), **1Q** and **1QCl** did not (Table 2, entries 3 and 4). This might indicate that the outer-sphere mechanism is facilitated or initiated in some fashion with base. In fact, a role of alkoxide base was recently discovered and rationalized by Gusev.[20] (b) We did not explore possible mechanisms that involve C−C bond coupling of the phosphine arm's methylene carbon to the ketone product carbonyl carbon atom.[9c] (c) Another notable phenomenon is that Milstein's catalyst was the only catalyst tested that can dehydrogenate 1-hexanol; the other catalysts were tested but did not dehydrogenate 1-hexanol. This may suggest a unique property of Milstein's catalyst, such as dehydroalkyation[24] or other unexpected reactivities, that our six catalysts do not possess.

CONCLUSIONS

We designed and used structurally analogous planar-locked quinoline ligands that do not have access to inner-sphere alcohol dehydrogenation mechanisms. The experimental results indicate that inhibiting amine arm dissociation negatively impacts the catalytic activity compared to systems that can operate through inner-sphere paths. We rationalized this on the basis that quinoline-derived pincer complexes (**1Q^{R}Cl**) must proceed through the energetic outer-sphere reaction profile, whereas the **Py** system has access to both paths, with the inner-sphere path calculated as being favorable.

According to literature and our computations, both inner- and outer-sphere paths share common Ru-bound alkoxide intermediates (**4a**). In the outer-sphere mechanism, these form as off-path species via isomerization of the key high-energy zwitterionic outer-sphere intermediate (**4b**). For the **Q^{R}** system, these Ru-bound alkoxides inhibit catalysis because they cannot progress to product through the inner-sphere steps and must isomerize back into the high energy zwitterionic intermediate. This contrasts the **Py** system that can progress to product through inner-sphere paths by its equivalent alkoxide intermediate. Hence, an additional explanation for the poor performance of **Q^{R}** system is the presence of low-energy off-path alkoxide intermediates (**4aQ^{R}**) resulting from their planar-locked nature.

Isoquinoline (**1Iso1QCl**), picoline (**1PCl**), and lutidine (**1LCl**) PNN and PN complexes were prepared to control for changes in aromatization/dearomatization chemistry. The three other complexes (**1Iso1QCl**, **1PCl**, and **1LCl**) had greater catalytic performance compared to that of **1Q^{R}Cl**, but they did not perform nearly as well as **1PyCl**. The mechanistic landscape of a single catalytic process can be dizzyingly complex with multiple pathways and connections between those pathways, and comparisons between multiple catalysts may be unreliable. While we have provided evidence to support a favored inner-sphere pathway for 1PhEtOH dehydrogenation with Milstein's catalyst (**1Py**), there are still other possibilities.

EXPERIMENTAL SECTION

General Methods. All reagents were purchased from commercial sources and used as received unless otherwise noted. Anhydrous solvents were dried and obtained from a PPT solvent purification system and stored over 3 Å molecule sieves inside of a glovebox (stabilizers in THF and diethyl ether are thus removed before use). Molecular sieves were activated at 200 °C under vacuum (<100 mTorr) for 3−4 days prior to use. HPLC-grade acetone was dried overnight over Na_2SO_4 and degassed with freeze−pump−thaw cycles. Organic syntheses were performed open to air unless otherwise noted. $Ru(PPh_3)_3(H)(CO)(Cl)$,[43] PyNP, and its complexes were prepared according to literature.[6] 1,3-Dimethylisoquinoline was prepared according to literature.[31] Ruthenium compounds were synthesized and manipulated under nitrogen in a VAC Genesis glovebox. NMR spectra were collected on a Varian Mercury-300 MHz or Inova-400 MHz spectrometers. FTIR-ATR spectra were collected inside of a VAC Atmospheres glovebox using a Bruker Alpha IR spectrometer with the "ATR Platinum" insert adapter (diamond crystal). UV−vis spectra were collected in an Agilent 8154 spectrophotometer. High-resolution mass spectrometry of precatalyst compounds was conducted in DCM using an FTICR Bruker 12 T mass spectrometer.

Crystallography. Low-temperature X-ray diffraction data for **1Q^{Ph}Cl** (Rlacy11, CCDC 1987652), **1Iso1QCl** (Rlacy40, CCDC 1987644), **1LCl** (Rlacy41, CCDC 1987647), **1QCl** (Rlacy42, CCDC 1987648), **1Q^{iPr}Cl** (Rlacy50, CCDC 1987649), and **1PCl** (Rlacy51, CCDC 1987651) (Supporting Information) were collected on a Rigaku XtaLAB Synergy diffractometer coupled to a Rigaku Hypix detector with either Mo Kα radiation (λ = 0.71073 Å) or Cu Kα radiation (λ = 1.54184 Å), from a PhotonJet microfocus X-ray source at 100 K. The diffraction images were processed and scaled using the CrysAlisPro software.[44] The structures were solved through intrinsic phasing using SHELXT[45] and refined against F^2,[46] on all data, by full-matrix least-squares with SHELXL[47] following established refinement strategies.[44] All non-hydrogen atoms were refined anisotropically. All hydrogen atoms bound to carbon were included in the model at geometrically calculated positions and refined using a riding model. The hydride H atoms were located on the difference map and refined upon freely. The isotropic displacement parameters of all (non-hydride) hydrogen atoms were fixed to 1.2 times the U_{eq} value of the atoms they are linked to (1.5 times for methyl groups).

Dehydrogenation Procedure. In a glovebox, a 25 or 50 mL Schlenk tube was charged with a fresh stir bar and 2 mL (0.0042 mmol, 0.5 mol %) of a stock solution of **1Py**, **1PyCl**, **1Q^{R}Cl** (R = ^{t}Bu, ^{i}Pr, and Ph), **1Q**, **1Iso1QCl**, **1PyCl**, **1PCl**, or **1LCl** in dry toluene via a syringe. To this solution was added 0.83 mmol of 1PhEtOH, and KO^{t}Bu (2 mg, 2 mol %) was added last. The apparatus was then sealed with a rubber septum and brought outside the glovebox where it was put under a positive pressure of argon via a Schlenk line. The tube was immersed in an oil bath that was heated beforehand to 110 °C and was vigorously stirred for 4 h. After 4 h, the reaction was allowed to cool room temperature and then immediately concentrated under a stream of air. Each catalyst was tested in triplicate when conversions were high or duplicate otherwise.[32] TD reactions were performed by the same procedure except that 1 mL of degassed and dried acetone was included in the mixture. No other byproducts were observed in resulting residues (Figure S55). After each experiment the tubes were washed with acetone, water, concentrated nitric acid, water, and acetone before placing them in an oven (~150 °C) for at least 1 h to remove residual water.

Determination of Percent Conversion. A ^{1}H NMR spectrum ($CDCl_3$) was taken of the resulting oil from the dehydrogenation reaction and the diagnostic peaks [(2.61 ppm, s (CH_3), acetophenone; 1.50 ppm, d (CH_3), J = 6.4 Hz, 1PhEtOH)] were integrated and summed to 100. The integration of the peak representing acetophenone was then taken as the percent conversion (Figure S55).

Computational Methods and Results. All calculations for the **Py** and **Q^{R}** (R = ^{t}Bu, ^{i}Pr, Ph) systems were performed using ORCA 4.2.1/Chemcraft 1.8 programs (see the Supporting Information for **Iso1Q**).[48] Geometry optimizations were performed in the solution phase at the PBE0/BSI level (BSI designates the basis set combination of def2-ECP for Ru[49] and def2-SVP[50] for nonmetal atoms) with solvation effects from toluene via the CPCM model[51] and dispersion effects from the Becke-Johnson damping scheme

https://dx.doi.org/10.1021/acs.organomet.0c00327
Organometallics 2020, 39, 3628−3644

(D3BJ).[52] Additionally, a larger integration grid was used (Grid4 in ORCA). Frequency calculations were performed to confirm the structures to be minima (no imaginary frequency) or transition states (one appropriate imaginary frequency). The energy results of the geometry calculations were further refined by performing single point energy (SPE) calculations at the PBE0/BSII level (BSII designates def2-ECP for Ru[49] and def2-TVPP[50] for nonmetal atoms). Solvation effects of toluene were calculated using the CPCM continuum solvent model.[51] Dispersion corrections were applied using the Becke-Johnson damping scheme (D3BJ).[52] A large integration grid was used (Grid5 in ORCA). IRC calculations were performed to ensure the transition states calculated connect the respective reactant to product. Standard state conversions (SSC) were applied to the final energies of each complex. Only reactions where the number of moles changed were corrected. For example, in association reactions $\Delta n = -1$, $R_1T\ln(R_2T^{\Delta n}) = -1.89$ kcal/mol (298 K) ($R_1 = 8.31447$ J K^{-1} mol^{-1}, $R_2 = 0.08206$ L atm K^{-1} mol^{-1}).[53]

The reaction coordinate for dehydrogenation of various alcohols and amines with **1Py** through β-hydride elimination and a stepwise outer-sphere has been investigated by others in the literature.[10−17] We replicated these reaction coordinates with **1Py**, **1Q^{R}** (R = ^{t}Bu, ^{i}Pr, and Ph), and **1Iso1Q**. The reaction coordinate diagram was normalized to the starting complexes' free energy (**1Py**, **1Q^{R}** (R = ^{t}Bu, ^{i}Pr, and Ph), **1Iso1Q**) and encompasses the net balanced reaction, with each step containing the free energies of the organometallic complex and the appropriate small molecule(s).

Synthesis of Quinoline-Derived Compounds. *Synthesis of 8-Nitro-2-methylquinoline.* The synthesis of 8-nitro-2-methylquinoline was achieved using a published procedure.[30] The resulting product was obtained in moderate yields (60−72%) and required no further purification.

Synthesis of 2-Methyl-8-aminoquinoline. A 100 mL round-bottomed flask was charged with 1.0 g (5.3 mmol) of 2-methyl-8-nitroquinoline, 95 mg (1.1 mmol) of 5% by wt Pd/C, and 10 mL of degassed EtOH under a flow of argon. The flask was evacuated and backfilled with H_2 via a balloon three times. The reaction was heated to 50 °C and stirred vigorously for 4 h, after which the flask was cooled to room temperature. The flask was then evacuated and backfilled with argon three times. The reaction was then quickly filtered through Celite open to air, and the resulting yellow filtrate was reduced to dryness in vacuo to a yellow oil. This oil readily changes color and was therefore used immediately in the following procedure. ^{1}H NMR spectra of the crude yellow oil matched those from commercial vendors and contained only the desired product.

Synthesis of N,N-Diethyl-2-methylquinolin-8-amine. A 500 mL round-bottomed flask was charged with freshly prepared 2-methyl-8-aminoquinoline 840 mg (5.3 mmol) and 60 mL of glacial acetic acid and then placed under an argon atmosphere. The reaction vessel was cooled to 0 °C, and 5 equiv (1.0 g, 26 mmol) of $NaBH_4$ was added slowly. After complete addition, the cold bath was removed, and the reaction was stirred for 1 h. Another 5 equiv (1.0 g, 26 mmol) of $NaBH_4$ was added slowly, and the reaction was then heated to 60 °C. After 1 h of stirring, another 5 equiv (1.0 g, 26 mmol) of $NaBH_4$ was added slowly at 60 °C. The reaction was stirred overnight at 60 °C, after which another 5 equiv (1.0 g, 26 mmol) of $NaBH_4$ was added slowly at 60 °C and stirred for 1 h. The reaction was cooled to room temperature and basified to ≥12 pH using 10 M NaOH open to air. The organic product was extracted with hexanes, and the combined organic layers were washed with brine and dried over Na_2SO_4. Concentration of the dried organic layer *in vacuo* gave a yellow oil which was purified by column chromatography (10% ethyl acetate in hexanes) to yield 248 mg (38%) of product. ^{1}H NMR (400 MHz, $CDCl_3$): δ, ppm 7.96 (d, J_{HH} = 8.4 Hz, 1H, quin-H7), 7.31 (qdt, J_{HH} = 4.6, 4.9, 5.4 Hz, 2H, quin-H4 quin-H6), 7.22 (d, J_{HH} = 8.4 Hz, 1H, quin-H3), 7.06 (dd, J_{HH} = 1.8, 7.2 Hz, 1H, quin-H5), 3.56 (q, J_{HH} = 7.0 Hz, 4H, N(CH_2CH_3)$_2$), 2.73 (s, 3H, quin−CH_3), 1.16 (t, J_{HH} = 7.0 Hz, 6H, N(CH_2CH_3)$_2$). ^{13}C{^{1}H} NMR (75 MHz, $CDCl_3$): δ, ppm 156.01 (s, quin-C2), 147.03 (s, quin-C8), 142.81 (s, quin-C8a), 136.43 (s, quin-C4), 127.87 (s, quin-C4a), 125.31 (s, quin-C6), 121.39 (s, quin-C7), 119.99 (s, quin-C3), 117.67 (s, quin-C5), 46.78 (s, N(CH_2CH_3)$_2$), 25.72 (s, quin-CH_3), 12.07 (s, N(CH_2CH_3)$_2$).

Synthesis of 2-((Ditertbutylphosphaneyl)methyl)-N,N-diethylquinolin-8-amine (QNP). In a nitrogen-filled glovebox, a 100 mL round-bottomed flask was charged with 100 mg (0.48 mmol) of *N,N*-diethyl-2-methylquinolin-8-amine and 10 mL of THF and cooled to 0 °C. Next, 190 μL of 2.5 M *n*-BuLi in hexanes was added to the round-bottomed flask dropwise via syringe with stirring at 0 °C, turning the yellow solution dark red. After the addition, the reaction was stirred for 1 h at 0 °C and then further cooled to −78 °C. A solution of 90 μL of P(^{t}Bu)$_2$Cl in 5 mL of THF was added dropwise with stirring at −78 °C. The resulting dark red solution was stirred overnight and allowed to warm to room temperature. The reaction was then brought out of the glovebox, and 10 mL of degassed water was added via syringe. The resulting organic product was extracted via cannula transfer into an argon-purged Erlenmeyer flask containing Na_2SO_4. The remaining aqueous layer was washed with degassed DCM (3 × 10 mL), and the organic products were combined and dried over the Na_2SO_4 under argon on a Schlenk line. Concentration *in vacuo* yielded an orange-red oil. This residue was brought into a nitrogen-filled glovebox, and no purification was needed, (149 mg, 89%). ^{31}P{^{1}H} NMR (121 MHz, $CDCl_3$): δ, ppm 34.99 (s). ^{1}H NMR (400 MHz, $CDCl_3$): δ, ppm 7.96 (d, J_{HH} = 8.5 Hz, 1H, quin-H7), 7.56 (d, J_{HH} = 8.5 Hz, 1H, quin-H3), 7.37−7.24 (m, 2H, quin-H4, quin-H6), 7.06 (dd, J_{HH} = 7.1, 1.9 Hz, 1H, quin-H5), 3.54 (q, J_{HH} = 7.1 Hz, 4H, N(CH_2CH_3)$_2$), 3.29 (d, J_{PH} = 3.8 Hz, 2H, CH_2P), 1.22−1.12 (m, 24H, P(C(CH_3)$_3$)$_2$), N(CH_2CH_3)$_2$).

Synthesis of 2-((Diphenylphosphaneyl)methyl)-N,N-diethylquinolin-8-amine (QNP^{Ph}). In a nitrogen-filled glovebox, 300 mg (1.4 mmol) of *N,N*-diethyl-2-methylquinolin-8-amine was dissolved in 10 mL of freshly dried THF. This solution was added to a 50 mL addition funnel, equipped with a flea stir bar, and placed on its side in a cold well chilled to 0 °C. To this solution, *n*-BuLi (558 μL 2.5 M hexanes, 1.4 mmol) was slowly added over the course of 5 min. The resulting dark red solution was stirred for 2 h at 0 °C and then cooled to −78 °C. In a separate round-bottomed flask, PPh_2Cl (0.250 mL, 1.4 mmol) was dissolved in 10 mL of THF and cooled to −78 °C. The red quinoline mixture was added to the PPh_2Cl solution dropwise over 30 min at −78 °C. After the addition, the reaction vessel was allowed to warm to room temperature with stirring overnight. The reaction vessel was then brought out of the glovebox and connect to a Schlenk line for anaerobic workup. To the reaction, 10 mL of degassed water was added, and the resulting organic layer was extracted via cannula transfer. The remaining aqueous layer was washed with DCM (3 × 10 mL), and the combined organic layers were dried over Na_2SO_4. This solution was transferred via cannula to an argon-filled Schlenk flask where it was concentrated under vacuum. The resulting residue was brought into a nitrogen-filled glovebox and purified by recrystallization from diethyl ether at −35 °C to yield off-white crystals (317 mg, 57%). ^{31}P{^{1}H} NMR (121 MHz, $CDCl_3$): δ, ppm −11.11 (s). ^{1}H NMR (400 MHz, $CDCl_3$): δ, ppm 7.91 (d, J_{HH} = 8.4 Hz, 1H, quin-H7), 7.49−7.44 (m, 4H, P(*o*-C_6H_5)$_2$), 7.35−7.21 (m, 9H, P(*m*-C_6H_5)$_2$, P(*p*-C_6H_5)$_2$), quin-H3, quin-H5, quin-H6), 7.02 (dd, J_{HH} = 1.5, 7.5 Hz, 1H, quin-H4), 3.86 (d, J_{PH} = 1.2 Hz, 2H, CH_2P), 3.44 (q, J_{HH} = 7.0 Hz, 4H, N(CH_2CH_3)$_2$), 1.19 (t, J_{HH} = 7.02 Hz, 6H, N(CH_2CH_3)$_2$). ^{13}C{^{1}H} NMR (75 MHz, $CDCl_3$): δ, ppm 155.48 (d, J_{PC} = 8.6 Hz, quin-C2)), 147.22 (s, quin-C8), 142.72 (s, quin-C8a), 138.35 (d, J_{PC} = 14.7 Hz, P(C_6H_5)), 136.58 (s, quin-C4), 132.91 (d, J_{PC} = 18.9 Hz, P(*o*-C_6H_5)), 128.52 (d, J_{PC} = 16.9 Hz, P(*m*-C_6H_5)), 128.32 (s, P(*p*-C_6H_5)), 128.11 (s, quin-C4a), 125.66, quin-C6), 121.47 (d, J_{PC} = 6.6 Hz, quin-C3), 119.71 (s, quin-C7), 117.53 (s, quin-C5), 46.46 (s, N(CH_2CH_3)$_2$), 40.06 (d, J_{PC} = 16.1 Hz, CH_2P), 12.18 (s, N(CH_2CH_3)$_2$).

Synthesis of 2-((Diisopropylphosphaneyl)methyl)-N,N-diethylquinolin-8-amine (QNP^{iPr}). QNP^{iPr} was synthesized using the same procedure as QNP with the exception of P(^{t}Bu)$_2$Cl being substituted for P(^{i}Pr)$_2$Cl. Purification was achieved by washing the resulting oil with diethyl ether (3 × 5 mL) to give 120 mg (78%) of product. ^{31}P{^{1}H} NMR (121 MHz, $CDCl_3$) δ, ppm 11.82 (s). ^{1}H NMR (300 MHz, $CDCl_3$) δ, ppm 7.97 (d, J_{HH} = 8.5 Hz, 1H, quin-H7), 7.44 (d,

https://dx.doi.org/10.1021/acs.organomet.0c00327
Organometallics 2020, 39, 3628−3644

J_{HH} = 8.5 Hz, 1H, quin-H3), 7.36−7.28 (m, 2H, quin-H4, quin-H6), 7.06 (d, J_{HH} = 7.1 Hz, 1H, quin-H5), 3.58 (q, J_{HH} = 7.0 Hz, 4H, $N(CH_2CH_3)_2$), 3.21 (d, J_{PH} = 2.9 Hz, 2H, CH_2P), 1.83 (qd, $J_{HH,\ PH}$ = 7.1, 2.0 Hz, 2H, $P(CH(CH_3)_2)_2$), 1.16 (t, J_{HH} = 7.0 Hz, 6H), 1.09 (t, J_{HH} = 6.9 Hz, 6H, $N(CH_2CH_3)_2$), 1.05 (dd, $J_{PH,\ HH}$ = 8.8, 7.1 Hz, 6H, $P(CH(CH_3)_2)_2$).

*Synthesis of (CO)(Cl)(H)(QNP)ruthenium(II) (**1QCl**).* In a nitrogen-filled glovebox, 50 mg (0.14 mmol) of QNP ligand and 130 mg (0.14 mmol) of $Ru(PPh_3)_3(H)(CO)(Cl)$ was mixed together in 4 mL of THF in a 25 mL sealed pressure vessel. The solution was stirred at 65 °C for 16 h, after which the reaction was filtered and the resulting filtrate concentrated *in vacuo* to ∼0.5 mL. Diethyl ether (2 mL) was added, and the resulting yellow/orange solid was collected on a glass-fritted funnel and washed with ether (3 × 5 mL) to yield 44 mg (60%). Crystals suitable for diffraction or further purification was obtained by recrystallization from DCM with diethyl ether diffusion. $^{31}P\{^1H\}$ NMR (121 MHz, $CDCl_3$): δ, ppm 111.04 (d, J_{PH} = 14.3 Hz). ^1H NMR (300 MHz, $CDCl_3$): δ, ppm 8.10 (d, J = 8.7 Hz, 1H, quin-H7), 7.69 (ddd, J_{HH} = 7.6, 6.3, 1.2 Hz, 2H, quin-H3, quin-H5), 7.59−7.47 (m, 2H, quin-H4, quin-H6), 4.37−4.24 (m, 1H, $N(CHHCH_3)_a$), 3.95−3.70 (m, 2H, CHHP, $N(CHHCH_3)_a$), 3.60 (dd, $J_{PH,\ HH}$ = 16.6, 10.9 Hz, 1H, CHHP), 3.24 (ddd, J_{HH} = 12.2, 7.0, 2.4 Hz, 1H, $N(CHHCH_3)_b$), 3.09−2.96 (m, 1H, $N(CHHCH_3)_b$), 1.78 (t, J_{HH} = 7.0 Hz, 3H, $N(CH_2CH_3)_a$), 1.49 (d, J_{PH} = 13.7 Hz, 9H, $P(C(CH_3)_3)_a$), 1.22 (d, J_{PH} = 13.1 Hz, 9H, $P(C(CH_3)_3)_b$), 1.05 (t, J_{HH} = 7.0 Hz, 3H, $N(CH_2CH_3)_b$)), −15.19 (d, J_{PH} = 25.9 Hz, 1H). FTIR-ATR: 1882 cm^{-1} (ν_{CO}). HRMS (FT-ICR-MS): $[(C_{22}H_{35}N_2P)(CO)(H)Ru]^+$ ($[M - Cl]^+$) $m/z_{(found)}$ = 489.160321, $m/z_{(calcd.)}$ = 489.16087.

*Synthesis of (CO)(Cl)(H)(QNP^{Ph})ruthenium(II) (**1Q^{Ph}Cl**).* In a nitrogen-filled glovebox, 64 mg (0.18 mmol) of QNP^{Ph} ligand and 170 mg (0.179 mmol) of $Ru(PPh_3)_3(H)(CO)(Cl)$ were mixed in 4 mL of THF in a 25 mL sealed pressure vessel. The solution was stirred at 65 °C for 12 h, after which the reaction was filtered. The resulting orange solid was collected on a glass-fritted funnel and washed with ether (3 × 5 mL) to yield 64 mg (63%) of a bright orange solid. Crystals suitable for diffraction were grown by layering a DCM solution under hexane. $^{31}P\{^1H\}$ NMR (121 MHz, $CDCl_3$): δ, ppm 74.51 (s). ^1H NMR (400 MHz, $CDCl_3$): δ, ppm 8.16 (d, J_{HH} = 8.6 Hz, 1H, quin-H7), 8.01−7.93 (m, 2H, $P(o\text{-}C_6H_5)_a$), 7.75 (d, J_{HH} = 8.2 Hz, 1H, quin-H5), 7.72 (d, J_{HH} = 7.4 Hz, 1H, quin-H4), 7.59 (t, J_{HH} = 8.9 Hz, 1H, quin-H6), 7.56 (d, J_{HH} = 7.8 Hz, 1H, quin-H3), 7.51−7.45 (m, 2H, $P(o\text{-}C_6H_5)_b$), 7.43−7.40 (m, 3H, $P(m\text{-}C_6H_5)_a$, $P(p\text{-}C_6H_5)_a$), 7.33−7.31 (m, 3H, $P(m\text{-}C_6H_5)_b$, $P(p\text{-}C_6H_5)_b$), 4.59 (dd, $J_{PH,\ HH}$ = 9.7, 18.4 Hz, 1H, CHHP), 4.40 (dd, $J_{PH,\ HH}$ = 12.2, 17.5 Hz, 1H, CHHP), 4.26 (ddd, J_{HH} = 7.0, 11.8, 14.3 Hz, 1H, $N(CHHCH_3)_a$), 3.81 (td, J_{HH} = 7.0, 19.5 Hz, 1H, $N(CHHCH_3)_a$), 3.35−3.23 (m, 1H, $N(CHHCH_3)_b$), 3.14−3.04 (m, 1H, $N(CHHCH_3)_b$), 1.83 (t, J_{HH} = 6.4 Hz, 3H, $N(CH_2CH_3)_a$), 1.09 (t, J_{HH} = 6.8 Hz, 3H, $N(CH_2CH_3)_b$), −14.14 (d, J_{PH} = 26.0 Hz, 1H, RuH). FTIR-ATR: 1909 cm^{-1} (ν_{CO}). HRMS (FT-ICR-MS): $[(C_{26}H_{27}N_2P)(CO)(H)Ru]^+$ ($[M - Cl]^+$) $m/z_{(found)}$ = 529.09746, $m/z_{(calcd.)}$ = 529.09772.

*Synthesis of (CO)(Cl)(H)(QNP^{iPr})ruthenium(II) (**1Q^{iPr}Cl**).* **1Q^{iPr}Cl** was synthesized using the same procedure as used for **1QCl**. Purification was achieved via recrystallization from DCM with diethyl ether layering to yield 38 mg (44%) of product. $^{31}P\{^1H\}$ NMR (121 MHz, $CDCl_3$): δ, ppm 100.80 (s). ^1H NMR (300 MHz, $CDCl_3$): δ, ppm 8.09 (d, J_{HH} = 8.4 Hz, 1H, quin-H7), 7.71 (d, J_{HH} = 7.8 Hz, 1H, quin-H3), 7.69 (d, J_{HH} = 7.2 Hz, 1H, quin-H4) 7.55 (t, J_{HH} = 7.8 Hz, 1H, quin-H6), 7.48 (d, J_{HH} = 8.5 Hz, 1H, quin-H5), 4.16 (dq, J_{HH} = 11.4, 7.2 Hz, 1H, $N(CHHCH_3)_a$), 3.84 (m, 2H, $N(CHHCH_3)_a$, CHHP), 3.60 (dd, J_{HH} = 17.2, 10.5 Hz, 1H, CHHP), 3.26 (m, 1H, $N(CHHCH_3)_b$), 3.11−2.86 (m, 2H, $N(CHHCH_3)_b$, $P(CH(CH_3)_2)_a$), 2.17 (dp, $J_{PH,\ HH}$ = 11.3, 6.7 Hz, 1H), $P(CH(CH_3)_2)_b$, 1.79 (t, J_{HH} = 7.0 Hz, 3H, $N(CH_2CH_3)_a$), 1.51 (dd, J_{HH} = 17.0, 7.4 Hz, 3H, $P(CH(CH_3)_a)_a$), 1.32 (dd, J_{HH} = 12.4, 7.2 Hz, 3H, $P(CH(CH_3)_b)_a$), 1.19−1.03 (m, 6H, $P(CH(CH_3)_a)_b$, $N(CH_2CH_3)_b$), 0.85 (dd, $J_{PH,\ HH}$ = 15.3, 6.8 Hz, 3H, $P(CH(CH_3)_b)_b$), −14.81 (d, J_{PH} = 23.6 Hz, 1H, RuH). FTIR-ATR: 1889 cm^{-1} (ν_{CO}). HRMS (FT-ICR-MS): $[(C_{20}H_{31}N_2P)(CO)(H)Ru]^+$ ($[M - Cl]^+$) $m/z_{(found)}$ = 461.129021, $m/z_{(calcd.)}$ = 461.12957.

*Synthesis of (CO)(H)(QNP′)ruthenium(II) (**1Q**).* In a nitrogen-filled glovebox, 39 mg (0.074 mmol) of **1QCl** was dissolved in 2 mL of THF in a 20 mL screw-capped vial. The solution was cooled to −35 °C, and 8 mg (0.074 mmol) of KO^{t}Bu was added. The resulting dark red solution was stirred at −35 °C for 4 h. Afterward, the reaction was filtered and the resulting filtrate was concentrated *in vacuo* to ∼0.5 mL. Petroleum ether (2 mL) was added and the resulting black solid was filtered off and discarded. The red filtrate was concentrated *in vacuo* to yield 29 mg (81%) of product. $^{31}P\{^1H\}$ NMR (121 MHz, C_7D_8): δ, ppm 98.7 (s). ^1H NMR (300 MHz, C_7D_8): δ, ppm 6.74 (dd, J_{HH} = 5.4, 3.3 Hz, 1H, quin-H7), 6.49 (s, 1H, quin-H3), 6.49 (s, 1H, quin-H5), 6.41 (d, J_{HH} = 2.0 Hz, 1H, quin-H6), 6.39 (s, 1H, quin-H4), 3.86 (d, J_{HH} = 2.3 Hz, 1H, CHP), 3.57−3.43 (m, 1H, $N(CHHCH_3)_a$), 3.24−3.08 (m, 1H, $N(CHHCH_3)_a$), 2.77 (dddd, J_{HH} = 11.7, 8.9, 7.0, 3.8 Hz, 2H, $N(CH_2CH_3)_b$), 1.32 (d, J_{PH} = 11.5 Hz, 9H, $P(C(CH_3)_3)_a$), 1.28 (d, J_{PH} = 12.0 Hz, 9H, $P(C(CH_3)_3)_a$), 1.07 (t, J_{HH} = 7.0 Hz, 3H, $N(CH_2CH_3)_a$), 0.50 (t, J_{HH} = 7.2 Hz, 3H, $N(CH_2CH_3)_b$), −25.02 (d, J_{PH} = 27.7 Hz, 1H). FTIR-ATR: 1897 cm^{-1} (ν_{CO}).

*Synthesis of (CO)(H)(QNP′^{Ph})ruthenium(II) (**1Q^{Ph}**).* The synthesis of **1Q^{Ph}** followed the same procedure as that for **1Q**, and 10 mg (71%) (15 mg, 0.02 mmol scale) of product was recovered as a dark red residue. $^{31}P\{^1H\}$ NMR (121 MHz, C_7D_8): δ, ppm 61.41 (d, J_{PH} = 12.9 Hz). ^1H NMR (300 MHz, C_7D_8) δ, ppm 7.95−7.83 (m, 2H, $P(o\text{-}C_6H_5)_a$), 7.85−7.73 (m, 2H, $P(o\text{-}C_6H_5)_b$), 7.13−6.93 (m, 7H, $P(m\text{-}C_6H_5)_2$, $(p\text{-}C_6H_5)_2$, quin-H7), 6.81 (dd, J = 6.4, 2.1 Hz, 1H, quin-H4), 6.62 (s, 1H, quin-H3), 6.51−6.41 (m, 2H, quin-H6, quin-H5), 4.33 (d, J_{PH} = 2.5 Hz, 1H, CHP), 3.53 (p, J_{HH} = 8.1, 7.3 Hz, 1H, $N(CHHCH_3)_a$), 3.12 (dt, J_{HH} = 14.1, 7.0 Hz, 1H, $N(CHHCH_3)_a$), 2.86 (td, J_{HH} = 7.3, 3.6 Hz, 2H, $N(CH_2CH_3)_b$), 0.96 (t, J_{HH} = 7.0 Hz, 3H, $N(CH_2CH_3)_a$), −0.01 (t, J_{HH} = 7.2 Hz, 3H, $N(CH_2CH_3)_b$), −22.70 (d, J = 34.0 Hz, 1H, RuH).

Synthesis of Isoquinoline-Derived Compounds. *Synthesis of 1-Bromomethyl-3-methylisoquinoline and 3-Bromomethyl-1-methylisoquinoline.* An argon-filled 250 mL two-necked round-bottomed flask equipped with a condenser was charged with 600 mg (3.82 mmol) of 1,3-dimethylisoquinoline, 50 mL of CCl_4, 687 mg (3.82 mmol) of NBS, and 93 mg (0.382 mmol) of benzoyl peroxide. The resulting mixture was stirred at 80 °C overnight. Afterward, the reaction was cooled to room temperature, and a tan solid was filtered off open to air. The filtrate was concentrated *in vacuo* and redissolved in 100 mL of benzene. This solution was washed with $NaHCO_3$ (3 × 50 mL) and brine (3 × 50 mL), and was dried over Na_2SO_4. Concentration *in vacuo* gave a dark orange oil with a roughly 50:50 mixture of each monobrominated isomer. Separation of the 3-bromo product was achieved using column chromatography (10% ethyl acetate in hexanes). *1-Bromomethyl-3-methylisoquinoline* (136 mg, 15%). ^1H NMR (300 MHz, $CDCl_3$): δ, ppm 8.20 (d, J_{HH} = 8.4 Hz, 1H, isoquin-H8), 7.77 (d, J_{HH} = 8.0 Hz, 1H, isoquin-H5), 7.69−7.64 (m, 1H, isoquin-H6), 7.64−7.55 (m, 1H, isoquin-H7), 7.47 (s, 1H, isoquin-H4), 5.02 (s, 2H, CH_2Br), 2.69 (s, 3H, isoquin−CH_3). *3-Bromomethyl-1-methylisoquinoline* (163 mg, 18%). ^1H NMR (300 MHz, $CDCl_3$): δ, ppm 8.12 (d, J_{HH} = 8.2 Hz, 1H, isoquin-H8), 7.79 (d, J_{HH} = 8.7 Hz, 1H, isoquin-H5), 7.67 (dt, J_{HH} = 8.1, 1.2 Hz, 1H, isoquin-H6), 7.63 (s, 1H, isoquin-H4), 7.59 (d, J_{HH} = 6.9 Hz, isoquin-H7), 4.70 (s, 2H, CH_2Br), 2.97 (s, 3H, isoquin-CH_3).

Synthesis of N-Ethyl-N-((1-methylisoquinolin-3-yl)methyl)-ethanamine. To a 50 mL round-bottomed flask open to air was charged 10 mL of THF and 120 mg (0.508 mmol) of the bromo methyl isoquinoline. The solution was then cooled to 0 °C before 0.12 mL (1.12 mmol) of diethylamine was added dropwise. The solution was stirred overnight and allowed to slowly warm to room temperature. The resulting suspension was concentrated *in vacuo*, and 50 mL of diethyl ether was added. This solution was washed with 3 × 15 mL 1 M NaOH and 3 × 15 mL saturated brine, and the combined organic layers were dried over Na_2SO_4. Concentration *in vacuo* provided mostly pure material, which was purified through column chromatography (75% ethyl acetate, hexanes) to give 53 mg (46%) of

https://dx.doi.org/10.1021/acs.organomet.0c00327
Organometallics 2020, 39, 3628−3644

N-ethyl-*N*-((3-methylisoquinolin-1-yl)methyl)ethanamine or 69 mg (59%) of *N*-ethyl-*N*-((1-methylisoquinolin-3-yl)methyl)ethanamine. *N-Ethyl-N-((1-methylisoquinolin-3-yl)methyl)ethanamine*: ^{1}H NMR (300 MHz, $CDCl_3$): δ, ppm 8.08 (d, J_{HH} = 8.7 Hz, 1H, isoquin-H8), 7.69 (d, J_{HH} = 8.0 Hz, 1H, isoquin-H5), 7.59 (t, J_{HH} = 7.4 Hz, 1H, isoquin-H6), 7.49 (t, J_{HH} = 8.4 Hz, 1H, isoquin-H7), 7.38 (s, 1H, isoquin-H4), 3.85 (s, 2H, $CH_2N(CH_2CH_3)_2$), 2.95 (s, 3H, isoquin−CH_3), 2.66 (q, J_{HH} = 7.5 Hz, 4H, $N(CH_2CH_3)_2$), 1.10 (t, J_{HH} = 7.1 Hz, 6H, $N(CH_2CH_3)_2$).

Synthesis of N-((1-((Ditert-butylphosphaneyl)methyl)-isoquinolin-3-yl)methyl)-N-ethylethanamine (1-P-IsoQNP). In a nitrogen-filled glovebox, a 100 mL round-bottomed flask was charged with 100 mg (0.44 mmol) of *N*-ethyl-*N*-((1-methylisoquinolin-3-yl)methyl)ethanamine and 10 mL of THF and cooled to 0 °C. The solution was treated with *n*-BuLi (175 μL of 2.5 M in hexanes, 0.44 mmol) dropwise with stirring at 0 °C, causing a color change from light to dark yellow. After the addition, the reaction was stirred for 1 h at 0 °C and was then further cooled to −78 °C. A solution of 83 μL (0.44 mmol) of $P(^tBu_2)Cl$ in 5 mL of THF was added dropwise with stirring at −78 °C. The resulting dark yellow solution was stirred overnight and allowed to warm to room temperature. The reaction was then brought out of the glovebox, and 10 mL of degassed water was added under an argon atmosphere. The resulting organic product was extracted via cannula transfer into an argon-purged Erlenmeyer flask containing Na_2SO_4. The remaining aqueous layer was washed with degassed DCM (3 × 10 mL), and the organic products were combined and dried over Na_2SO_4. Concentration *in vacuo* yielded an orange oil. This residue was brought into a nitrogen-filled glovebox, and no further purification was needed (146 mg, 90%). $^{31}P\{^1H\}$ NMR (121 MHz, $CDCl_3$): δ, ppm 34.92 (s). ^{1}H NMR (300 MHz, $CDCl_3$): δ, ppm 8.45 (d, J_{HH} = 8.3 Hz, 1H, isoquin-H8), 7.75 (d, J_{HH} = 8.1 Hz, 1H, isoquin-H5), 7.60 (s, 1H, isoquin-H4), 7.57−7.48 (m, 2H, isoquin-H6, isoquin-H7), 3.84 (s, 2H, $CH_2N(CH_2CH_3)_2$), 3.65 (s, 2H, CH_2P), 2.65 (q, J_{HH} = 6.9 Hz, 4H, $N(CH_2CH_3)_2$), 1.17 (d, J_{PH} = 10.8 Hz, 18H, $P(C(CH_3)_3)_2$), 1.10 (t, J_{HH} = 7.2 Hz, 6H, $N(CH_2CH_3)_2$).

*Synthesis of (CO)(Cl)(H)(1-P-IsoQNP)ruthenium(II) (**1Iso1QCl**).* In a nitrogen-filled glovebox, 50 mg (0.13 mmol) of 1-P-IsoQNP ligand and 121 mg (0.127 mmol) of $Ru(PPh_3)_3(H)(CO)(Cl)$ were mixed in 4 mL of THF in a 25 mL sealed pressure vessel. The solution was stirred at 65 °C for 16 h, after which the reaction was filtered. The resulting filtrate was concentrated *in vacuo* to ∼0.5 mL. Diethyl ether (2 mL) was added, and the resulting yellow/orange solid was isolated on a glass-fritted funnel and washed with diethyl ether (3 × 5 mL) to yield 64 mg (93%) of clean product. Crystals suitable for diffraction were obtained by from DCM with hexane diffusion. $^{31}P\{^1H\}$ NMR (121 MHz, $CDCl_3$): δ, ppm 107.01 (d, J_{HH} = 22.0 Hz). ^{1}H NMR (300 MHz, $CDCl_3$): δ, ppm 8.12 (d, J_{HH} = 8.3 Hz, 1H, isoquin-H8), 7.79 (dd, J_{HH} = 8.2, 1.5 Hz, 1H, isoquin-H5), 7.72 (ddd, J_{HH} = 8.1, 6.7, 1.2 Hz, 1H, isoquin-H6), 7.64 (ddd, J_{HH} = 8.2, 6.5, 1.6 Hz, 1H, isoquin-H7), 7.53 (s, 1H, isoquin-H4), 5.44 (d, J_{HH} = 12.5 Hz, 1H, C*H*HN), 4.08 (dd, $J_{PH,\ HH}$ = 17.3, 9.3 Hz, 1H, C*H*HP), 4.01−3.85 (m, 1H, $N(CHHCH_3)_a$), 3.81 (dd, J_{HH} = 14.1, 2.8 Hz, 1H, CH*H*N), 3.58 (dd, J_{HH} = 14.1, 7.1 Hz, 1H, $N(CHHCH_3)_a$), 3.38 (dd, $J_{PH,\ HH}$ = 17.3, 8.2 Hz, 1H, CH*H*P), 2.77 (q, J_{HH} = 6.7 Hz, 2H, $N(CH_2CH_3)_b$), 1.41 (d, J_{PH} = 13.6 Hz, 9H, $P(C(CH_3)_3)_a$), 1.35 (d, J_{PH} = 13.1 Hz, 9H, $P(C(CH_3)_3)_b$), 1.26 (t, J_{HH} = 7.0 Hz, 3H, $N(CH_2CH_3)_a$), 1.13 (t, J_{HH} = 7.2 Hz, 3H, $N(CH_2CH_3)_b$), −15.55 (d, J_{PH} = 27.7 Hz, 1H, Ru*H*). FTIR-ATR: 1898 cm^{-1} (ν_{CO}). HRMS (FT-ICR-MS): $[(C_{23}H_{37}N_2P)(CO)(H)Ru]^+$ ($[M - Cl]^+$) $m/z_{(found)}$ = 503.175971, $m/z_{(calcd.)}$ = 503.17652.

Synthesis of Pyridine-Derived Compounds. *Synthesis of 2-((Ditert-butylphosphaneyl)methyl)pyridine (PicP).* In a nitrogen-filled glovebox, a 100 mL round-bottomed flask was charged with 1.0 g (10.74 mmol) of 2-picoline and 10 mL of diethyl ether and cooled to 0 °C. The picoline solution was subsequently treated with 4.3 mL of 2.5 M *n*-BuLi in hexanes. After the addition, this solution was stirred at 0 °C for 1 h before being cooled further to −78 °C. A solution of 2.0 mL (10.74 mmol) of P^tBu_2Cl in 10 mL of diethyl ether was added dropwise at −78 °C. After the addition, this solution was stirred overnight and allowed to slowly warm to room temperature. The reaction was then brought out of the glovebox, and 10 mL of degassed water was added under an argon atmosphere. The resulting organic product was extracted via cannula transfer into an argon-purged Erlenmeyer flask containing Na_2SO_4. The remaining aqueous layer was washed with degassed DCM (3 × 10 mL), and the organic products were combined and dried over Na_2SO_4. Separation by cannula transfer and concentration *in vacuo* yielded an orange oil. Vacuum distillation (<10 mmTorr) yielded a colorless oil (bp 88 °C) which was pure product, (2.3 g, 92%). $^{31}P\{^1H\}$ NMR (121 MHz, $CDCl_3$): δ, ppm 36.24 (s). ^{1}H NMR (300 MHz, $CDCl_3$): δ, ppm 8.45 (d, J_{HH} = 5.0 Hz, 1H, py-H6), 7.56 (dt, J_{HH} = 7.8, 1.9, 1.3 Hz, 1H, py-H4), 7.43 (d, J_{HH} = 7.2 Hz, 1H, py-H3), 7.03 (t, J_{HH} = 6.8, 6.0 Hz, 1H, py-H5), 3.04 (d, J_{HH} = 3.4 Hz, 2H, CH_2P), 1.13 (d, J_{PH} = 10.9 Hz, 18H, $P(C(CH_3)_3)_2$).

Synthesis of 2-((Ditert-butylphosphaneyl)methyl)-6-methylpyridine (LutP). In a nitrogen-filled glovebox, a 100 mL round-bottomed flask was charged with 200 mg (1.86 mmol) of 2,6-lutidine and 5 mL of diethyl ether and cooled to 0 °C. The lutidine solution was subsequently treated with 746 μL of 2.5 M *n*-BuLi in hexanes. After the addition, this solution was stirred at 0 °C for 1 h before being cooled further to −78 °C. A solution of 355 μL (1.86 mmol) of P^tBu_2Cl in 5 mL of diethyl ether was added dropwise at −78 °C. After the addition, this solution was stirred overnight and allowed to slowly warm to room temperature. The reaction was then brought out of the glovebox, and 10 mL of degassed water was added under an argon atmosphere. The resulting organic product was extracted via a cannula transfer into an argon-purged Erlenmeyer flask containing Na_2SO_4. The remaining aqueous layer was washed with degassed DCM (3 × 10 mL) and the organic products were combined and dried over Na_2SO_4. Separation by cannula transfer and concentration *in vacuo* yielded a pale yellow solid. Passing this yellow solid through a plug of alumina using petroleum ether gave a white solid after concentration *in vacuo*, which was pure product (443 mg, 95%). $^{31}P\ \{^1H\}$ NMR (121 MHz, $CDCl_3$): δ, ppm 35.26. ^{1}H NMR (300 MHz, $CDCl_3$): δ, ppm 7.44 (t, J_{HH} = 7.7 Hz, 1H, py-H4), 7.28 (d, J_{HH} = 7.7 Hz, 1H, py-H3), 6.89 (d, J_{HH} = 7.6 Hz, 1H, py-H5), 3.03 (d, J_{PH} = 3.4 Hz, 2H, CH_2P), 2.49 (s, 3H, py-CH_3), 1.13 (d, J_{PH} = 11.0 Hz, 18H, $P(C(CH_3)_3)_2$). $^{13}C\ \{^1H\}$ NMR (75 MHz, $CDCl_3$): δ, ppm 136.18 (py-C4), 120.85 (s, py-C3), 120.71 (s, py-C5), 119.88 (s, py-C3), 119.86 (s, py-C6), 31.60 (d, J_{PC} = 10.3 Hz, $P(C(CH_3)_3)_a$), 29.64 (d, J_{PC} = 13.2 Hz, $P(C(CH_3)_3)_b$), 29.64 (d, J_{PC} = 13.2 Hz, py-CH_2P), 24.49 (s, $P(C(CH_3)_3)_2$).

*Synthesis of (CO)(Cl)(H)(PicP)(PPh_3)ruthenium(II) (**1PCl**).* In a nitrogen-filled glovebox, 50 mg (0.42 mmol) of PicP ligand and 360 mg (0.379 mmol) of $Ru(PPh_3)_3(H)(CO)(Cl)$ were mixed in 4 mL of THF in a 25 mL sealed pressure vessel. The solution was stirred at 65 °C for 16 h, after which the reaction was filtered and the resulting filtrate was concentrated *in vacuo* to ∼0.5 mL. Petroleum ether (2 mL) was added slowly, and the resulting solid was filtered and washed with petroleum ether (3 × 5 mL) to yield 92 mg (73%) of clean product. Crystals suitable for diffraction were obtained from DCM/petroleum ether. $^{31}P\{^1H\}$ NMR (121 MHz, $CDCl_3$): δ, ppm 98.71 (d, J_{PH} = 280 Hz, $P(^tBu)_2$), 37.58 (d, J_{PH} = 273 Hz, PPh_3). ^{1}H NMR (300 MHz, $CDCl_3$): δ, ppm 7.95 (d, J_{HH} = 5.7 Hz, 1H, py-H6), 7.67 (td, J_{HH} = 7.4, 3.5 Hz, 6H, $P(o\text{-}(C_6H_5)_3)$), 7.41−7.12 (m, 11H, py-H4, py-H3, $P(m\text{-}(C_6H_5)_3)$, $P(p\text{-}(C_6H_5)_3)$), 6.41 (t, J_{HH} = 6.6 Hz, 1H, py-H5), 3.57−3.43 (m, 1H, C*H*HP), 3.37 (dd, $J_{PH,\ HH}$ = 16.1, 7.3 Hz, 1H, CH*H*P), 1.33 (dd, J_{PH} = 56.5, 13.3 Hz, 18H, $P(C(CH_3)_3)_2$), −14.46 (dd, J_{PH} = 23, 22 Hz, 1H, Ru*H*). FTIR-ATR: 1916 cm^{-1} (ν_{CO}). HRMS (FT-ICR-MS): $[(C_{14}H_{24}NP)(PPh_3)(CO)(H)Ru]^+$ ($[M - Cl]^+$) $m/z_{(found)}$ = 630.162309, $m/z_{(calcd.)}$ = 630.16286.

*Synthesis of (CO)(Cl)(H)(LutP)(PPh_3) ruthenium(II) (**1LCl**).* In a nitrogen-filled glovebox, 100 mg (0.398 mmol) of LutP ligand and 360 mg (0.318 mmol) of $Ru(PPh_3)_3(H)(CO)(Cl)$ were mixed in 4 mL of THF in a 25 mL sealed pressure vessel. The solution was stirred at 65 °C for 16 h, after which the reaction was filtered. The resulting filtrate was concentrated *in vacuo* to ∼0.5 mL. Petroleum ether (2 mL) was added, and the resulting solid was filtered and washed with petroleum ether (3 × 5 mL) to yield 145 mg (67%) of

https://dx.doi.org/10.1021/acs.organomet.0c00327
Organometallics 2020, 39, 3628−3644

clean product. Crystals suitable for diffraction were obtained from DCM/petroleum ether. $^{31}P\{^{1}H\}$ NMR (121 MHz, $CDCl_3$): δ, ppm 92.25 (d, J_{PH} = 280 Hz), 35.69 (d, J_{PH} = 280 Hz). ^{1}H NMR (300 MHz, $CDCl_3$): δ, ppm 7.61 (t, J_{HH} = 8.4 Hz, 6H, P(*o*-(C_6H_5)$_3$)), 7.43−7.13 (m, 11H, py-H4, py-H3, P(*m*-(C_6H_5)$_3$), P(*p*-(C_6H_5)$_3$))), 6.62 (d, J_{HH} = 7.6 Hz, 1H, py-H5), 3.84−3.69 (m, 1H, C*H*HP), 3.57 (dd, $J_{PH, HH}$ = 16.1, 7.5 Hz, 1H, CH*H*P), 2.52 (s, 3H, py−CH_3), 1.32 (d, J_{PH} = 12.9 Hz, 18H, P(C(CH_3)$_3$))), −14.79 (dd, J_{PH} = 28.2, 18.8 Hz, 1H, Ru*H*). FTIR-ATR: 1924 cm^{-1} (ν_{CO}). HRMS (FT-ICR-MS): $[(C_{15}H_{26}NP)(PPh_3)(CO)(H)Ru]^+$ ($[M - Cl]^+$) $m/z_{(found)}$ = 644.177959, $m/z_{(calcd.)}$ = 644.17851.

*Synthesis of (CO)(H)(LutP)(PPh$_3$)ruthenium(II) (**1L**).* In a nitrogen-filled glovebox, 15 mg (0.022 mmol) of **1LCl** was dissolved in ∼0.75 mL of C_7D_8 in a 20 mL screw-capped vial. To this solution was added 2.5 mg (0.022 mmol) of KO^{t}Bu. The resulting dark green solution was stirred at room temperature overnight. Afterward, the forest green solution was charged to a screw-capped NMR tube. $^{31}P\{^{1}H\}$ NMR (121 MHz, C_7D_8): δ, ppm 118.16 (d, J_{PH} = 235 Hz), 54.76 (d, J_{PH} = 234 Hz). ^{1}H NMR (300 MHz, C_7D_8): δ, ppm 7.63 (ddd, J_{HH} = 10.0, 6.6, 3.0 Hz, 6H, P(*o*-(C_6H_5)$_3$)), 7.03−6.87 (m, 9H, P(*m*-(C_6H_5)$_3$), P(*p*-(C_6H_5)$_3$)), 6.55 (t, J_{HH} = 7.7 Hz, 1H, py-H4), 5.80 (d, J_{HH} = 7.7 Hz, 1H, py-H3), 5.74 (d, J_{HH} = 7.8 Hz, 1H, py-H5), 1.67 (d, J_{PH} = 3.3 Hz, 1H, C*H*P), 1.62 (s, 3H, py−CH_3), 1.32 (d, J_{PH} = 13.5 Hz, 9H, P(C(CH_3)$_3$)$_a$), 1.07 (d, J_{PH} = 13.4 Hz, 9H, P(C(CH_3)$_3$)$_b$), −14.34 (dd, J_{PH} = 22.5, 19.1 Hz, 1H, Ru*H*). FTIR-ATR: 1897 cm^{-1} (ν_{CO}).

■ ASSOCIATED CONTENT

Supporting Information

The Supporting Information is available free of charge at https://pubs.acs.org/doi/10.1021/acs.organomet.0c00327.

NMR, IR, and UV−vis spectra, DFT figures (PDF)

Cartesian coordinates of the calculated structures (XYZ)

Accession Codes

CCDC 1987644, 1987647−1987649, and 1987651 contain the supplementary crystallographic data for this paper. These data can be obtained free of charge via www.ccdc.cam.ac.uk/data_request/cif, or by emailing data_request@ccdc.cam.ac.uk, or by contacting The Cambridge Crystallographic Data Centre, 12 Union Road, Cambridge CB2 1EZ, UK; fax: +44 1223 336033.

■ AUTHOR INFORMATION

Corresponding Author

David C. Lacy − *Department of Chemistry, University at Buffalo, SUNY, Buffalo, New York 14260-3000, United States;* orcid.org/0000-0001-5546-5081; Email: DCLacy@Buffalo.edu

Authors

Paul M. Fanara − *Department of Chemistry, University at Buffalo, SUNY, Buffalo, New York 14260-3000, United States*

Samantha N. MacMillan − *Department of Chemistry and Chemical Biology, Cornell University, Ithaca, New York 14853, United States;* orcid.org/0000-0001-6516-1823

Complete contact information is available at: https://pubs.acs.org/10.1021/acs.organomet.0c00327

Notes

The authors declare no competing financial interest.

■ ACKNOWLEDGMENTS

Financial support was provided by the University at Buffalo (UB) start-up funds, an ACS Petroleum Research Fund (ACS-PRF-57861-DN13), and an NSF CAREER award (1847933). This work was completed using the resources of the UB Chemistry Instrument Center (CIC). Support was also provided by the Center for Computational Research at the University at Buffalo.

■ REFERENCES

(1) Shvo, Y.; Czarkie, D.; Rahamim, Y.; Chodosh, D. F. A new group of ruthenium complexes: structure and catalysis. *J. Am. Chem. Soc.* **1986**, *108*, 7400−7402.

(2) Conley, B. L.; Pennington-Boggio, M. K.; Boz, E.; Williams, T. J. Discovery, applications, and catalytic mechanisms of Shvo's catalyst. *Chem. Rev.* **2010**, *110*, 2294−2312.

(3) Gunanathan, C.; Milstein, D. Applications of acceptorless dehydrogenation and related transformations in chemical synthesis. *Science* **2013**, *341*, 1229712.

(4) (a) Kuriyama, W.; Matsumoto, T.; Ogata, O.; Ino, Y.; Aoki, K.; Tanaka, S.; Kobayashi, T.; Sayo, N.; Saito, T.; Saito, T. Catalytic hydrogenation of esters. Development of an efficient catalyst and processes for synthesising (R)-1,2-propanediol and 2-(l-menthoxy)-ethanol. *Org. Process Res. Dev.* **2012**, *16*, 166−171. (b) Nielsen, M.; Alberico, E.; Baumann, W.; et al. Low-temperature aqueous-phase methanol dehydrogenation to hydrogen and carbon dioxide. *Nature* **2013**, *495*, 85−89. (c) Oldenhuis, N. J.; Dong, V. M.; Guan, Z. Catalytic acceptorless dehydrogenations: Ru-Macho catalyzed construction of amides and imines. *Tetrahedron* **2014**, *70*, 4213−4218. (d) Zhang, L.; Nguyen, D. H.; Raffa, G.; Trivelli, X.; Capet, F.; Desset, S.; Paul, S.; Dumeignil, F.; Gauvin, R. M. Catalytic conversion of alcohols into carboxylic acid salts in water: scope, recycling, and mechanistic insights. *ChemSusChem* **2016**, *9*, 1413. (e) Li, H.; Wang, X.; Wen, M.; Wang, Z.-X. Computational insight into the mechanism of selective imine formation from alcohol and amine catalyzed by the ruthenium(II)-PNP pincer complex. *Eur. J. Inorg. Chem.* **2012**, *2012*, 5011−5020. (f) Shu, S.; Huang, M.; Jiang, J.; Qu, L.-B.; Liu, Y.; Ke, Z. Catalyzed or non-catalyzed: chemoselectivity of Ru-catalyzed acceptorless dehydrogenative coupling of alcohols and amines via metal−ligand bond cooperation and (de)aromatization. *Catal. Sci. Technol.* **2019**, *9*, 2305−2314. (g) Zeng, M.; Li, L.; Herzon, S. B. A highly active and air-stable ruthenium complex for the ambient temperature *anti*-Markovnikov reductive hydration of terminal alkynes. *J. Am. Chem. Soc.* **2014**, *136*, 7058−7067. (h) Ye, Z.; Huang, X.; Shao, Y.; Jiang, J.; Qu, L.-B.; Zhao, C.; Ke, Z. One catalyst, multiple processes: ligand effects on chemoselective control in Ru-catalyzed *anti*-Markovnikov reductive hydration of terminal alkynes. *Catal. Sci. Technol.* **2019**, *9*, 2315−2327. (i) Dub, P. A.; Batrice, R. J.; Gordon, J. C.; Scott, B. L.; Minko, Y.; Schmidt, J. G.; Williams, R. F. Engineering catalysts for selective ester hydrogenation. *Org. Process Res. Dev.* **2020**, *24*, 415−442. (j) Filonenko, G. A.; Aguila, M. J. B.; Schulpen, E. N.; Van Putten, R.; Wiecko, J.; Müller, C.; Lefort, L.; Hensen, E. J. M.; Pidko, E. A. Bis-N-heterocyclic carbene aminopincer ligands enable high activity in ru-catalyzed ester hydrogenation. *J. Am. Chem. Soc.* **2015**, *137*, 7620−7623. (k) Spasyuk, D.; Smith, S.; Gusev, D. G. Replacing phosphorus with sulfur for the efficient hydrogenation of esters. *Angew. Chem., Int. Ed.* **2013**, *52*, 2538−2542.

(5) Selected reviews: (a) Crabtree, R. H. Homogeneous transition metal catalysis of acceptorless dehydrogenative alcohol oxidation: applications in hydrogen storage and to heterocycle synthesis. *Chem. Rev.* **2017**, *117*, 9228−9246. (b) Younus, H. A.; Su, W.; Ahmad, N.; Chen, S.; Verpoort, F. Ruthenium pincer complexes: synthesis and catalytic applications. *Adv. Synth. Catal.* **2015**, *357*, 283−330. (c) Werkmeister, S.; Neumann, J.; Junge, K.; Beller, M. Pincer-Type complexes for catalytic (de)hydrogenation and transfer (de)hydrogenation reactions: recent progress. *Chem. - Eur. J.* **2015**, *21*, 12226−12250. (d) Werkmeister, S.; Junge, K.; Beller, M. Catalytic hydrogenation of carboxylic acid esters, amides, and nitriles with homogeneous catalysts. *Org. Process Res. Dev.* **2014**, *18*, 289−302. (e) Eisenstein, O.; Crabtree, R. H. Outer sphere hydrogenation catalysis. *New J. Chem.* **2013**, *37*, 21−27. (f) Grützmacher, H.

Cooperating ligands in catalysis. *Angew. Chem., Int. Ed.* **2008**, *47*, 1814−1818.
(6) Zhang, J.; Leitus, G.; Ben-David, Y.; Milstein, D. Facile conversion of alcohols into esters and dihydrogen catalyzed by new ruthenium complexes. *J. Am. Chem. Soc.* **2005**, *127*, 10840−10841.
(7) Gunanathan, C.; Milstein, D. Metal−ligand cooperation by aromatization−dearomatization: a new paradigm in bond activation and "green" catalysis. *Acc. Chem. Res.* **2011**, *44*, 588−602.
(8) Khusnutdinova, J. R.; Milstein, D. Metal−ligand cooperation. *Angew. Chem., Int. Ed.* **2015**, *54*, 12236−12273.
(9) (a) With water: Kohl, S. W.; Weiner, L.; Schwartsburd, L.; Konstantinovski, L.; Shimon, L. J. W.; Ben-David, Y.; Iron, M. A.; Milstein, D. Consecutive thermal H_2 and light-induced O_2 evolution from water promoted by a metal complex. *Science* **2009**, *324*, 74−77. (b) With MeOH: Balaraman, E.; Gunanathan, C.; Zhang, J.; Shimon, L. J. W.; Milstein, D. Efficient hydrogenation of organic carbonates, carbamates and formates indicates alternative routes to methanol based on CO_2 and CO. *Nat. Chem.* **2011**, *3*, 609−−614. (c) With Benzyl alcohol and EtOH: Montag, M.; Zhang, J.; Milstein, D. Aldehyde binding through reversible C−C coupling with the pincer ligand upon alcohol dehydrogenation by a PNP−ruthenium catalyst. *J. Am. Chem. Soc.* **2012**, *134*, 10325−10328.
(10) Li, H.; Wang, X.; Huang, F.; Lu, G.; Jiang, J.; Wang, Z. Computational study on the catalytic role of pincer ruthenium(II)-PNN complex in directly synthesizing amide from alcohol and amine: the origin of selectivity of amide over ester and imine. *Organometallics* **2011**, *30*, 5233−5247.
(11) Song, C.; Qu, S.; Tao, Y.; Dang, Y.; Wang, Z.-X. DFT mechanistic study of Ru^{II}-catalyzed amide synthesis from alcohol and nitrile unveils a different mechanism for borrowing hydrogen. *ACS Catal.* **2014**, *4*, 2854−2865.
(12) Qu, S.; Dang, Y.; Song, C.; Wen, M.; Huang, K.-W.; Wang, Z.-X. Catalytic mechanisms of direct pyrrole synthesis via dehydrogenative coupling mediated by PNP-Ir or PNN-Ru pincercomplexes: crucial role of proton-transfer shuttles in the PNP-Ir system. *J. Am. Chem. Soc.* **2014**, *136*, 4974−4991.
(13) Li, H. X.; Hall, M. B. Mechanism of the formation of carboxylate from alcohols and water catalyzed by a bipyridine-based ruthenium complex: a computational Study. *J. Am. Chem. Soc.* **2014**, *136*, 383−395.
(14) Cho, D.; Ko, K. C.; Lee, J. Y. Catalytic mechanism for the ruthenium-complex-catalyzed synthesis of amides from alcohols and amines: a DFT study. *Organometallics* **2013**, *32*, 4571−4576.
(15) Li, H.; Wen, M.; Wang, Z. X. Computational mechanistic study of the hydrogenation of carbonate to methanol catalyzed by the Ru^{II}PNN complex. *Inorg. Chem.* **2012**, *51*, 5716−5727.
(16) Zeng, G.; Li, S. Insights into dehydrogenative coupling of alcohols and amines catalyzed by a (PNN)-Ru(II) hydride complex: unusual metal-ligand cooperation. *Inorg. Chem.* **2011**, *50*, 10572−10580.
(17) Hou, C.; Zhang, Z.; Zhao, C.; Ke, Z. FT Study of acceptorless alcohol dehydrogenation mediated by ruthenium pincer complexes: ligand tautomerization governing metal ligand cooperation. *Inorg. Chem.* **2016**, *55*, 6539−6551.
(18) Johnson, J. B.; Bäckvall, J.-E. Mechanism of ruthenium-catalyzed hydrogen transfer reactions. concerted transfer of OH and CH hydrogens from an alcohol to a (cyclopentadienone)ruthenium complex. *J. Org. Chem.* **2003**, *68*, 7681−7684.
(19) (a) Dub, P. A.; Gordon, J. C. The role of the metal-bound N−H functionality in Noyori-type molecular catalysts. *Nat. Rev. Chem.* **2018**, *2*, 396−408. (b) Dub, P. A.; Gordon, J. C. Metal-ligand bifunctional catalysis: the "accepted" mechanism, the issue of concertedness, and the function of the ligand in catalytic cycles involving hydrogen atoms. *ACS Catal.* **2017**, *7*, 6635−6655.
(20) Gusev, D. Revised mechanisms of the catalytic alcohol dehydrogenation and ester Reduction with the Milstein PNN complex of ruthenium. *Organometallics* **2020**, *39*, 258−270.
(21) (a) Sandoval, C. A.; Ohkuma, T.; Muñiz, K.; Noyori, R. Mechanism of asymmetric hydrogenation of ketones catalyzed by BINAP/1,2-diamine−ruthenium(II) complexes. *J. Am. Chem. Soc.* **2003**, *125*, 13490−13503. (b) Dub, P. A.; Henson, N. J.; Martin, R. L.; Gordon, J. C. Unravelling the mechanism of the asymmetric hydrogenation of acetophenone by [RuX_2(diphosphine)(1,2-diamine)] catalysts. *J. Am. Chem. Soc.* **2014**, *136*, 3505−3521. (c) Dub, P. A.; Scott, B. L.; Gordon, J. C. Why does alkylation of the N−H functionality within M/NH bifunctional Noyori-type catalysts lead to turnover? *J. Am. Chem. Soc.* **2017**, *139*, 1245−1260. (d) Dub, P. A.; Gordon, J. C. The mechanism of enantioselective ketone reduction with Noyori and Noyori−Ikariya bifunctional catalysts. *Dalton Trans.* **2016**, *45*, 6756−6781. (e) Dub, P. A.; Henson, N. J.; Martin, R. L.; Gordon, J. C. Unravelling the mechanism of the asymmetric hydrogenation of acetophenone by [RuX_2(diphosphine)(1,2-Diamine)] catalysts. *J. Am. Chem. Soc.* **2014**, *136*, 3505−3521.
(22) Casey, C. P.; Singer, S. W.; Powell, D. R.; Hayashi, R. K.; Kavana, M. Hydrogen transfer to carbonyls and imines from a hydroxycyclopentadienyl ruthenium hydride: evidence for concerted hydride and proton transfer. *J. Am. Chem. Soc.* **2001**, *123*, 1090−1100.
(23) Tseng, K.-N. T.; Kampf, J. W.; Szymczak, N. K. Mechanism of *N,N,N*-amide ruthenium(II) hydride mediated acceptorless alcohol dehydrogenation: inner-sphere β-H elimination versus outer-sphere bifunctional metal−ligand cooperativity. *ACS Catal.* **2015**, *5*, 5468−5485.
(24) He, T.; Buttner, J. C.; Reynolds, E. F.; Pham, J.; Malek, J. C.; Keith, J. M.; Chianese, A. R. Dehydroalkylative activation of CNN- and PNN-pincer ruthenium catalysts for ester hydrogenation. *J. Am. Chem. Soc.* **2019**, *141*, 17404−17413.
(25) Cherepakhin, V.; Williams, T. J. Iridium catalysts for acceptorless dehydrogenation of alcohols to carboxylic acids: scope and mechanism. *ACS Catal.* **2020**, *10*, 56−65.
(26) Cherepakhin, V.; Williams, T. J. Catalyst evolution in ruthenium-catalyzed coupling of amines and alcohols. *ACS Catal.* **2020**, *10*, 56−65.
(27) (a) Zhang, L.; Peng, D.; Leng, X.; Huang, Z. Iron-catalyzed, atom-economical, chemo- and regioselective alkene hydroboration with pinacolborane. *Angew. Chem., Int. Ed.* **2013**, *52*, 3676−3680. (b) Speiser, F.; Braunstein, P.; Saussine, L. New nickel ethylene oligomerization catalysts bearing bidentate P,N-phosphinopyridine ligands with different substituents α to phosphorus. *Organometallics* **2004**, *23*, 2625−2632. (c) Li, H.; Fiorito, D.; Mazet, C. Exploring site selectivity of iridium hydride insertion into allylic alcohols: serendipitous discovery and comparative study of organic and organometallic catalysts for the vinylogous Peterson elimination. *ACS Catal.* **2017**, *7*, 1554−1562. (d) Grice, K. A.; Goldberg, K. I. Insertion of dioxygen into a platinum(II)−methyl bond to form a platinum(II) methylperoxo complex. *Organometallics* **2009**, *28*, 953−955. (e) Beddie, C.; Wei, P.; Stephan, D. W. Titanium pyridylphosphinimide complexes. Synthesis, structure, and ethylene polymerization catalysis. *Can. J. Chem.* **2006**, *84*, 755−761. (f) Gerald, E. P.; Andrew, F. I.; Stuart, Y. B. Heterocycle-containing phosphines & their use as ligands in palladium catalysed coupling reactions. GB2378182 (A), February 2, 2005.
(28) (a) Yang, H.; Lugan, N. I.; Mathieu, R. Study of the bonding properties of the new ligands $C_5H_3N(2\text{-}R')(6\text{-}CH_2PPhR)$ toward rhodium(I). Evidence for a dynamic competition for bonding between O- and N-donor centers when R = o-anisyl, R' = Me. *Organometallics* **1997**, *16*, 2089. (b) Devillard, M.; Lamsfus, C. A.; Vreeken, V.; Maron, L.; Van Der Vlugt, J. I. Versatile coordination of a reactive P,N-ligand toward boron, aluminum and gallium and interconversion reactivity. *Dalton Trans.* **2016**, *45*, 10989−10998. (c) De Boer, S. Y.; Gloaguen, Y.; Lutz, M.; Van Der Vlugt, J. I. Cu-I click catalysis with cooperative noninnocent pyridylphosphine ligands. *Inorg. Chim. Acta* **2012**, *380*, 336−342. (d) De Boer, S. Y.; Gloaguen, Y.; Reek, J. N. H.; Lutz, M.; van der Vlugt, J. I. N−H bond activation by palladium(II) and copper(I) complexes featuring a reactive bidentate PN-ligand. *Dalton Trans.* **2012**, *41*, 11276−11283. (e) Jongbloed, L. S.; De Bruin, B.; Reek, J. N. H.; Lutz, M.; Van Der Vlugt, J. I. Reversible cyclometalation at RhI as a motif for

https://dx.doi.org/10.1021/acs.organomet.0c00327
Organometallics 2020, 39, 3628−3644

metal−ligand bifunctional bond activation and base-free formic acid dehydrogenation. *Catal. Sci. Technol.* **2016**, *6*, 1320−1327.
(29) [{PicP}Ru(cymene)Cl] has been used in catalyzed alkylation of amines: Celaje, J. A.; Zhang, X.; Zhang, F.; Kam, L.; Herron, J. R.; Williams, T. J. A base and solvent-free ruthenium-catalyzed alkylation of amines. *ACS Catal.* **2017**, *7*, 1136−1142.
(30) Madeja, V. K. An improved method of synthesizing ortho- and para-substituted methyl-1, 10-phenanthroline. *J. Prakt. Chem.* **1962**, *17*, 97−103.
(31) Sato, T.; Tamura, K.; Nagayoshi, K. A convenient synthetic method of 1,3-disubstituted isoquinolines using silver trifluoromethanesulfonate as a key reagent. *Chem. Lett.* **1983**, *12*, 791−794.
(32) Inclusion of Hg in **1PyCl** and Ru(H)(CO)(Cl)(PPh_3)$_3$ 1PhEtOH dehydrogenation reactions gave identical results.
(33) **Ru** is a known alcohol dehydrogenation catalyst. Selected examples: (a) Tsuji, Y.; Kotachi, S.; Huh, K.-T.; Watanabe, Y. Ruthenium-catalyzed dehydrogenative N-heterocyclization. Indoles from 2-aminophenethyl alcohols and 2-nitrophenethyl alcohols. *J. Org. Chem.* **1990**, *55*, 580−584. (b) Ray, R.; Chandra, S.; Maiti, D.; Lahiri, G. K. Simple and efficient ruthenium-catalyzed oxidation of primary alcohols with molecular oxygen. *Chem. - Eur. J.* **2016**, *22*, 8814−8822.
(34) **Ru** is a known alpha-alcohol TD catalyst. Kuwahara, T.; Fukuyama, T.; Ryu, I. RuHCl(CO)(PPh_3)$_3$-catalyzed α-alkylation of ketones with primary alcohols. *Org. Lett.* **2012**, *14*, 4703−4705.
(35) (a) Attempts to optimize intermediates **3** and **4** and certain transition states for **1L** and **1P** could not be located unless PPh_3 was removed in silico and therefore are not included in this work. (b) The DFT calculations for **Iso1Q** were performed using different methodology and not used in the mechanistic comparison (see the Supporting Information).
(36) Bootsma, J.; Guo, B.; de Vries, J. G.; Otten, E. Ruthenium complexes with PNN pincer ligands based on (chiral) pyrrolidines: synthesis, structure, and dynamic stereochemistry. *Organometallics* **2020**, *39*, 544−555.
(37) Iron, M. A.; Ben-Ari, E.; Cohen, R.; Milstein, D. Metal−ligand cooperation in the trans addition of dihydrogen to a pincer Ir(I) complex: a DFT study. *Dalton Trans.* **2009**, 9433−9439.
(38) (a) Chakraborty, S.; Lagaditis, P. O.; Forster, M.; Bielinski, E. A.; Hazari, N.; Holthausen, M. C.; Jones, W. D.; Schneider, S. Well defined iron catalysts for the acceptorless reversible dehydrogenation-hydrogenation of alcohols and ketones. *ACS Catal.* **2014**, *4*, 3994−4003. (b) Yang, X. Mechanistic insights into Ruthenium catalyzed production of H_2 and CO_2 from methanol and water: A DFT Study. *ACS Catal.* **2014**, *4*, 1129−−1133.
(39) Smith, N. E.; Bernskoetter, W. H.; Hazari, N. The role of proton shuttles in the reversible activation of hydrogen via metal-ligand cooperation. *J. Am. Chem. Soc.* **2019**, *141*, 17350−17360.
(40) Hasanayn, F.; Morris, R. H. Symmetry aspects of H_2 splitting by five-coordinate d^6 ruthenium amides, and calculations on acetophenone hydrogenation, ruthenium alkoxide formation, and subsequent hydrogenolysis in a model *trans*-Ru(H)$_2$(diamine)-(diphosphine) system. *Inorg. Chem.* **2012**, *51*, 10808−10818.
(41) The conversion of **2Py** into **1Py** (benzene, room temperature) took nearly 2 days to reach ∼25% completion and was largely unaffected by inclusion of 10 mol % 1PhEtOH. This contrasts the rapid conversion of **2Py** into **1Py** when stoichiometric acetone was present and resulted in a 1:1 ratio of **1Py** to isopropanol. Our rationale is that the TD process is downhill relative to acetone and **2Py**, whereas the alcohol-assisted process is uphill. Nevertheless, the alcohol-assisted mechanism may very well be important under conditions relevant to catalytic alcohol dehydrogenation, which are at elevated temperatures and H_2 is being removed from the headspace.
(42) Other structural parameters (e.g., *d*, percent buried volume, phosphine cone angle) showed poor to no correlation to conversions and/or calculated transition state energies or $\Delta G^{\ddagger}$ when compared across all seven complexes.
(43) Ahmad, N.; Levison, J. J.; Robinson, S. D.; Uttley, M. F.; Wonchoba, E. R.; Parshall, G. W. Complexes of Ruthenium, Osmium, Rhodium, and Iridium Containing Hydride Carbonyl, or Nitrosyl Ligands. *Inorg. Synth.* **2007**, *15*, 45−64.
(44) *CrysAlisPro*; Rigaku OD, The Woodlands, TX, 2015.
(45) Sheldrick, G. M. SHELXT − Integrated space-group and crystal-structure determination. *Acta Crystallogr., Sect. A: Found. Adv.* **2015**, *A71*, 3−8.
(46) Sheldrick, G. M. A short history of SHELX. *Acta Crystallogr., Sect. A: Found. Crystallogr.* **2008**, *A64*, 112−122.
(47) Müller, P. Practical suggestions for better crystal structures. *Crystallogr. Rev.* **2009**, *15*, 57−83.
(48) (a) Neese, F. The ORCA program system. *Wiley Interdiscip. Rev.: Comput. Mol. Sci.* **2012**, *2*, 73−78. (b) Neese, F. Software update: the ORCA program system, version 4.0. *Wiley Interdiscip. Rev.: Comput. Mol. Sci.* **2018**, *8*, e1327.
(49) Andrae, D.; Haeussermann, U.; Dolg, M.; Stoll, H.; Preuss, H. Energy-adjusted *ab initio* pseudopotentials for the second and third row transition elements. *Theor. Chim. Acta* **1990**, *77*, 123−141.
(50) Weigend, F.; Ahlrichs, R. Balanced basis sets of split valence, triple zeta valence and quadruple zeta valence quality for H to Rn: Design and assessment of accuracy. *Phys. Chem. Chem. Phys.* **2005**, *7*, 3297.
(51) Barone, V.; Cossi, M. Quantum calculation of molecular energies and energy gradients in solution by a conductor solvent model. *J. Phys. Chem. A* **1998**, *102*, 1995.
(52) (a) Grimme, S.; Ehrlich, S.; Goerigk, L. Effect of the damping function in dispersion corrected density functional theory. *J. Comput. Chem.* **2011**, *32*, 1456−1465. (b) Grimme, S.; Antony, J.; Ehrlich, S.; Krieg, H. A consistent and accurate ab initio parametrization of density functional dispersion correction (DFT-D) for the 94 elements H-Pu. *J. Chem. Phys.* **2010**, *132*, 154104.
(53) Cramer, C. J. *Essentials of Computational Chemistry: Theories and Models*; John Wiley & Sons Ltd, 2002; p 183.

https://dx.doi.org/10.1021/acs.organomet.0c00327
Organometallics 2020, 39, 3628−3644